Tbilisi State University
High Energy Physics Institute

Deuteron Polarimetry Studies at COSY–Jülich with the ANKE Spectrometer

Diploma Thesis of
David Chiladze

Head of Faculty	Prof. I. Tevzadze
Adviser, Tbilisi	Prof. M. Nioradze
Advisers, Jülich	Dr. A. Kacharava
	Dr. F. Rathmann
Referee, London	Prof. C. Wilkin

Diploma work carried out at the
Institut für Kernphysik
Forschungszentrum Jülich GmbH
2004

Contents

Abstract

Nuclear reactions induced by beams of 1.2 GeV vector and tensor polarized deuterons incident on a hydrogen cluster target have been studied in a test experiment at the ANKE magnetic spectrometer, which is situated inside the COSY-Jülich storage ring. By measuring precisely the momenta of one or two final charged particles it was possible to identify clearly the processes $\vec{d}p \to dp$ and $\vec{d}p \to {}^3\mathrm{He}\,\pi^0$, both of which have large and well determined analyzing powers in our kinematic region. A preliminary analysis of these data thus allowed us to extract values for the vector and tensor polarizations of the beam. These are compared to the values measured using the EDDA polarimeter at lower beam energies and much lower intensities.

The primary reaction that will be studied in later runs will be that of $\vec{d}p \to (pp)n$ at small momentum transfers leading to a proton-proton pair at low excitation energy. In order to measure the differential cross section and tensor analyzing power of the charge-exchange reaction with reasonable error bars, and thus to reconstruct directly the magnitudes of at least two of the spin-dependent amplitudes with an accuracy sufficient to have an impact upon the Nucleon-Nucleon data bases, it is necessary to provide the experiment with a good determination of luminosity and polarimetry of the beam. The investigation will be carried out up to the maximum COSY energy, but the procedures have already been verified during the present test at lower energies by extracting the value of the tensor analyzing power in the forward direction, which is consistent with theoretical predictions. ANKE is therefore ready to embark on a programme of polarized deuteron physics. These aspects of the proposed study at the ANKE spectrometer are the main subject of the current diploma work.

The results given in this diploma work was presented by author on the nuclear physics spring meeting at university of Cologne (DPG meeting, March 8-12, 2004) and are included in the invited talk "Spin Physics of NN interactions at COSY" at spin physics symposium (SPIN2004, October 10-16, Trieste).

1 Introduction

1.1 Physics case

The nucleon-nucleon (NN) interaction represents one of the simplest and most fundamental systems involving the strong force. An appreciation of the NN interaction constitutes a necessary step towards a consistent understanding of the binding of neutrons and protons in nuclei, as well as giving an insight into reactions between nucleons (or nuclei) and nuclei and, most importantly, into the make-up of nuclear matter.

The complete description of the NN interaction requires precise data, in particular from double-polarization experiments [1], for phase–shift analyzes (PSA) from which the scattering amplitudes can be reconstructed.

For the pp system such complete experiments were carried out up to beam energies of about 3.0 GeV [2, 3], whereas much less information is available on spin observables in elastic np scattering, especially above 800 MeV [4, 5]. The PSA results for the isospin $I = 0$ NN system are thus poorly tested experimentally and measurements of any observable at small angles are highly desirable in order to check the validity of the PSA solutions for np amplitudes and, if necessary improve these solutions.

Information on the spin–dependent np elastic amplitudes near the backward direction (the charge–exchange region) can be obtained by measuring the Charge–Exchange (CE) break up of polarized deuterons on hydrogen. The sum of the amplitudes of the spin–dependent parts of the elementary $np \to pn$ CE amplitude can then be inferred from the probability of the dp CE process. Furthermore, it has been shown [6, 7] that, by measuring the deuteron tensor Analysing powers, it is possible to separate the intensities of the different spin amplitudes.

Under special kinematic conditions (scattering angle θ close to zero and momentum transfer between neutron and proton $t \sim 0$), and in impulse approximation, the dp CE differential cross section is fully determined by the spin–dependent parts of the elementary $np \to pn$ amplitude. A measurement of the differential cross section and the tensor analysing power T_{20} will allow us to extract directly the $|\beta|^2$ and $|\varepsilon|^2$ intensities of the spin-flip amplitudes [8] .

1.2 Study of *np* system at ANKE

The challenging physics goals of the np program at ANKE comprise the following objectives ($see\ \ http://www.fz-juelich.de/ikp/anke/doc/Proposals.html$):

1. Substantial and systematic enhancement of the world database of pn elastic scattering through a series of high-precision experiments, using polarized protons quasi-elastically scattered off the polarized deuteron target ($\vec{p}\vec{d}$).

2. Measurement of the spin structure of the amplitudes of the elementary np charge-exchange (CE) process via deuteron-induced reactions ($\vec{d}\vec{p}$).

The experimental programme is divided into two parts:

1. The first stage will utilise unpolarized and tensor and vector polarized deuteron beams incident on an unpolarized hydrogen cluster target. The differential cross section gives the overall intensity of the spin–dependent parts of the elementary CE process. The tensor polarised beam then enables us to separate the absolute values of two spin–dependent amplitudes.

2. Using transversely polarized deuterons incident on a polarized internal hydrogen gas target and measuring the spin–correlation coefficient opens the possibility of obtaining the relative phases between amplitudes.

Since we plan to measure the cross section in parallel with polarization observables, our experiment will be the first that can provide complete data necessary to determine the spin-dependent part of the elementary np process in the energy range above LAMPF (800 MeV) up to the maximum beam energy per nucleon (1150 MeV) achievable at COSY. The ANKE spectrometer is sensitive to the angular range of $\theta_{c.m.} \approx 0° - 30°$, which is unchartered territory for the pn system.

The first test experiment was done at COSY–Jülich with the ANKE Spectrometer in November 2003 with a polarized deuteron beam of energy T_d=1.2 GeV (p_d = 2.4 GeV/c). The aim of the run was to carry out a feasibility test of the experiment and to develop the polarimetry of the COSY deuteron beam using the ANKE spectrometer alone, which is very important for future polarization experiments at COSY and may replace the EDDA detector [3] for polarimetry in the long run.

In order to measure the differential cross section and T_{20} of the charge-exchange reaction with reasonable error bars, and thus to reconstruct directly the magnitudes of at least two of the spin-dependent amplitudes with an accuracy sufficient to have an impact upon the Nucleon-Nucleon data bases, it is necessary to provide the experiment with a good determination of luminosity and polarimetry of the beam.

1.3 Types of polarization experiments

Nuclear scattering and reaction experiments, with the known or measured spin polarization of one of the participant particles are the following types [9]:

(i) $A(b, \vec{c})D$ polarization experiments;

(ii) $A(\vec{b}, c)D$ analysing power experiments.

An experiment of type (i) implies the use of some sort of device to measure the polarization of the outgoing particles; this is normally done by observing an asymmetry, such as a ‘left - right’ asymmetry, in a further nuclear reaction or scattering.

An experiment of type (ii) involves the observation of the effects, again such as a left-right asymmetry, of a projectile beam whose polarization is known on the reaction or scattering of interest. In the early days the simplest polarization experiments involved a ‘double scattering’ process: the first scattering produced a polarized beam of particles, and the azimuthal angular distribution of the second scattering gave information about the polarization of the once scattered beam and about the analysing power of the second scattering or reaction. Double scattering experiments necessarily involve relatively low counting rates, so most of them lead to poor energy and angular resolution, and are thus limited to studies of processes with relatively large cross sections.

The development of polarized ion sources and polarized targets has considerably simplified experiments involving the measurement of Analysing powers. These developments permit experiments in which the spin polarizations of two of the reactants are measured. Experiments of this sort are:

(iii) $A(\vec{b},\vec{c})D$ polarization - transfer experiments;

(iv) $\vec{A}(\vec{b},c)D$ spin - correlation (initial channel) experiments;

(v) $A(b,\vec{c}\vec{d})$ spin - correlation (final channel) experiments.

An experiment of type (iii) is sometimes called a 'triple - scattering experiment', in deference to the experimental technique involved before polarized ion sources were available. That is, the first scattering was used to polarize the beam, the second was that studied, and a third was used to analyze the polarization of the final particles. With a polarized ion source this reduced to a double scattering.

A type (iv) experiment involves both polarized beams and polarized targets. Polarized thermal neutrons and suitable polarized targets for their use have been available for some time. More recently polarized targets suitable for fast neutrons and to some extent for charged particles have become available. These, together with the relatively intense polarized particle beams now available, make experiments of this type quite feasible in many cases of interest in nuclear physics.

An experiment of type (v) involves the simultaneous measurement of the polarization of both final particles. There have been no significant breakthroughs in methods for analysing the polarization of particle beams, so these experiments remain as difficult as ever and have not been done except for nucleon-nucleon scattering. In the case of elastic scattering, however, time reversal invariance, if valid, relates experiments of type (v) to equivalent experiments of type (iv).

In this thesis we will discuss an experiment of type (ii).

2 Principles of polarization

In quantum mechanics all spin angular momentum operators S_i satisfy the equation:

$$S_iS_j - S_jS_i = \epsilon_{ijk}S_k \tag{1}$$

These spin operators are hermitian and their trace is 0. We have three components in a Cartesian coordinate system S_x, S_y, and S_z which defines the vector $\vec{S}$. Their eigenvalues and eigenfunctions satisfy:

$$\vec{S}^2\left|sm\right\rangle = s\left(s+1\right)\hbar\left|sm\right\rangle \tag{2}$$

$$S_z\left|sm\right\rangle = m\hbar\left|sm\right\rangle \;\; m=-s,-s+1,...,+s \tag{3}$$

$\left|sm\right\rangle$ is the eigenfunction of $\vec{S}^2$ and one of its projection, conventionally chosen to be the z projection. It depends on two quantum numbers: spin quantum number s and magnetic quantum number m. The number of values of m is $(2s+1)$.

When $s = 1/2$, we then have two values $m = -1/2$ or $m = +1/2$. We can write the spin operator in terms of matrices with the Pauli definition:

$$\vec{S} = \tfrac{1}{2}\hbar\vec{\sigma} \tag{4}$$

where

$$\begin{aligned}\sigma_x &= \begin{pmatrix} 0 & 1 \\ 1 & 0 \end{pmatrix}\\ \sigma_y &= \begin{pmatrix} 0 & -i \\ i & 0 \end{pmatrix}\\ \sigma_z &= \begin{pmatrix} 1 & 0 \\ 0 & -1 \end{pmatrix}\end{aligned} \tag{5}$$

The set of these three Pauli matrices and unit matrix form a complete set of hermitian matrices for $s = 1/2$. Every hermitian operator in these space is linear combination of these operators. This representation is very useful in quantum mechanics.

2.1 Spin 1/2

The above describes a single particle with $\langle S_z\rangle = \pm 1/2\cdot\hbar$ and corresponding $\langle\sigma_z\rangle = \pm 1$. It is, however, impossible to describe things in such a way when there is ensemble of particles (for example a beam). To represent such ensemble in quantum mechanics, it is convenient to define the density matrix:

$$\rho = \sum_{i=1}^{n} p_i\left|sm_i\right\rangle\left\langle sm_i\right| \tag{6}$$

With:
$n \equiv$ number of the pure states (here $n = 2$);
$p_i \equiv$ probability of i state in the ensemble.

It helps to describe polarization with three components p_i $(i = x, y, z)$ which are the expectation values of the Pauli operators $\langle\sigma_i\rangle$. We can write it in the short way:

$$p_i = \langle\sigma_i\rangle = \mathrm{Trace}\left(\rho\sigma_i\right) \tag{7}$$

These are the components of a vector $\vec{p} = (p_x, p_y, p_z)$. The polarization $\vec{p}$ is the vector polarization of the ensemble of particles with spin 1/2. Here we should be carefully because in quantum mechanics only one component can be measured. Taking this to be the z-component:

$$p_z^* = \langle \sigma_z \rangle = \mathrm{Trace}\,(\rho \sigma_z) = p_+ \langle + | \sigma_z | + \rangle + p_- \langle - | \sigma_z | - \rangle = p_+ - p_- \tag{8}$$

When $p_z^* = 0$, it means that $p_+ = p_-$ and the probabilities of $|1/2, +1/2\rangle$ and $|1/2, -1/2\rangle$ states are equal. The state with $m = +1/2$ is populated with the same number of particles N_+ as the $m = -1/2$ states N_-.

If $p_+ > p_-$, it means that there are more particles in state $|1/2, +1/2\rangle$, and $N_+ > N_-$. So we have polarization along the z axis:

$$p_z^* = p_+ - p_- = \frac{N_+}{N_{tot}} - \frac{N_-}{N_{tot}} = \frac{N_+ - N_-}{N_+ + N_-}, \tag{9}$$

from which we evidently get:

$$-1 \leq p_z^* \leq +1. \tag{10}$$

If all particles in the beam are in the state $m = 1/2$, then we get polarization of the beam $p_z^* = 1$, or if all particles are in the state $m = -1/2$, we have $p_z^* = -1$.

2.2 Measurement of vector polarization

In the quantum-mechanical consideration of the beam theory, the polarization of the particles in the beam may affect the differential cross section of a nuclear reaction.

In the theory of polarized beams, the transfer- or M-matrix is generaly used instead of the scattering amplitudes f of the unpolarized particles. The cross section for a polarized spin-$\frac{1}{2}$ particles may be written:

$$\left(\frac{d\sigma}{d\Omega}\right)_{pol} = \left(\frac{d\sigma}{d\Omega}\right)_0 \left(1 + p_x A_x + p_y A_y + p_z A_z\right), \tag{11}$$

where $\left(\frac{d\sigma}{d\Omega}\right)_0$ is the cross section for scattering with an unpolarized beam. A_i is the "analysing power" or "efficiency tensor" (of rank one) of the reaction. Beside the type of nuclear reaction, the A_i depend on the beam energy and the angle ϑ, between the momentum k_{in} of incident and k_{out} outgoing particles. The analysing powers A_i are defined by:

$$A_i = A_i\,(E, \theta) = \frac{\mathrm{Trace}\left(M\ \sigma_i\ M^\dagger\right)}{\mathrm{Trace}\left(M\ M^\dagger\right)} \quad \text{for} \quad i = x, y, z. \tag{12}$$

Because of parity conservation, the reaction is sensitive only to the component of A_i which is normal to the scattering plane. According to the Madison convention of 1970, the axis of this coordinate system are fixed as follows:

$$\vec{z} \parallel \vec{k}_{in} \quad (13)$$
$$\vec{y} \parallel \vec{k}_{in} \times \vec{k}_{out} \quad (14)$$
$$\vec{x} \parallel \vec{y} \times \vec{z} \quad (15)$$

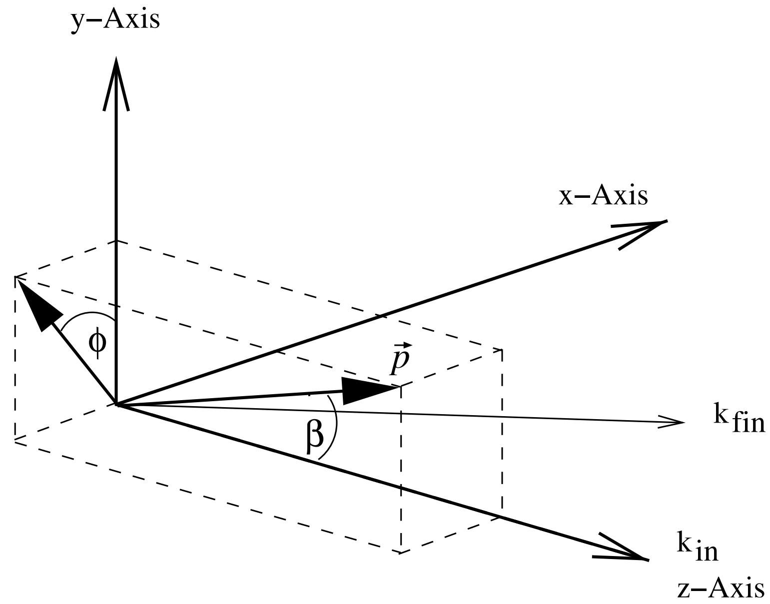

Figure 1: Madison convention for the definition of the laboratory-coordinate system

Also, according to this convention, every detector defines its own coordinate system through the different direction of the momentum k_{out}. Only the z axis has the same direction (in all coordinate systems). The unit vector pointing along the spin quantization axis is denoted by $\vec{p}$. Its direction is defined in terms of the angles β and ϕ, as shown in Fig. 1. β measures the angle between the quantization axis and the beam direction, while ϕ measures the angle between the projection of $\vec{p}$ in the x, y plane and the y axis. The sense of ϕ is important and is positive, as illustrated in Fig. 1. The advantage of this definition is that the x- and z- axes are in the scattering plane and, as already mentioned, only $A_y \neq 0$. Eq. (11) thereby simplifies to:

$$\left(\frac{d\sigma}{d\Omega}\right)_{pol} = \left(\frac{d\sigma}{d\Omega}\right)_0 (1 + p_y A_y) = \left(\frac{d\sigma}{d\Omega}\right)_0 (1 + p_z^* \sin\beta \cos\phi A_y) \,. \quad (16)$$

Besides the p_z^* is the measurable vector polarization along the polarization $\vec{p}$. In case of the $\beta = 90^\circ$ and $\phi = 0^\circ$, the polarization vector $\vec{p}$ is along the y axis and $p_y = p_z^* = |\vec{p}|$. In all other cases, all components of the polarization should be calculated, for example as $p_y = p_z^* \sin\beta\cos\phi$.

Beside the representation of the polarization in a Cartesian coordinate system, there is also a description in terms of spherical coordinates in the literature [9].

According to the Madison convention, if the azimuthal angle $\phi = 0$, scattering is to the left (L), and if $\phi = 180^\circ$, scattering is to the right (R). The angle between beam and scattered particle is ϑ. So, for the counts we will have:

$$L_{(\theta,\beta,\phi)} = n\ N_A\ \Omega_L\ \mathcal{E} \left(\frac{d\sigma}{d\Omega}\right)_{(\theta)} (1 + p_y A_y) \tag{17}$$

$$R_{(\theta,\beta,\phi)} = n\ N_A\ \Omega_R\ \mathcal{E} \left(\frac{d\sigma}{d\Omega}\right)_{(\theta)} (1 - p_y A_y) \tag{18}$$

$L_{(\theta,\beta,\phi)} \equiv$ Number of the particles measured in the left detector;
$R_{(\theta,\beta,\phi)} \equiv$ Number of the particles measured in the right detector;
$n \equiv$ Number of the incicdent particles;
$N_A \equiv$ Number of the target particles;
$\Omega_i \equiv$ Solid angle of the detector;
$\mathcal{E} \equiv$ Efficiency of the detector;
$\sigma_0 \equiv$ Cross section for unpolarized particles.

To measure the polarization there are two possibilities:

- For the first case we can flip the analyzer by rotating the analyzer 180° around the beam direction and counting again Spin-'Up' ($\uparrow$) and Spin-'Down' ($\downarrow$) particles. We then calculate left-right asymmetry:

$$\epsilon_1 := \sqrt{\frac{L\uparrow \cdot R\downarrow}{R\uparrow \cdot L\downarrow}} = \frac{1 + p_y A_y}{1 - p_y A_y} \tag{19}$$

  For the polarization we get:

$$p_y = \frac{\epsilon - 1}{\epsilon + 1} \cdot \frac{1}{A_y} \tag{20}$$

- By the comparison of polarized and unpolarized runs, one can achieve the same goal

$$\epsilon_2 = \frac{L_{pol} R_{unpol}}{L_{unpol} R_{pol}} = \frac{1 + p_y A_y}{1 - p_y A_y} \qquad \text{and} \qquad p_y = \frac{\epsilon - 1}{\epsilon + 1} \cdot \frac{1}{A_y} \tag{21}$$

One can notice that in the calculations of the error Δp_y, contributions from these observables: n, N_A, Ω_i, $\mathcal{E}$ and $\left(\frac{d\sigma}{d\Omega}\right)_0$ are very small. Only analysing power and asymmetry ϵ gives significant contributions to the error of the polarization:

$$\Delta p \sim \Delta A \cdot \Delta\epsilon \tag{22}$$

For this reason the first possibility of measuring polarization is better than the second one since:

$$\Delta p_{\epsilon_2} = \sqrt{2} \Delta p_{\epsilon_1} \tag{23}$$

If one uses directly the measured 'L' and 'R' in the Eq. (20) instead of ϵ and assumes that the counts depend primarily on the cross section of the reaction (because $n, N_A, \mathcal{E}$ and Ω_i are mostly fixed in the experiment) we will get for the errors:

$$\Delta p \sim \frac{1}{A\sqrt{L+R}} \propto \frac{1}{A} \cdot \frac{1}{\sqrt{t\left(\frac{d\sigma}{d\Omega}\right)_0}}, \tag{24}$$

Where: t is the measurement time. Therefore, one can define a figure of merit as:

$$A^2 \cdot \left(\frac{d\sigma}{d\Omega}\right)_0 \tag{25}$$

The bigger this term is, the smaller the measurement time t to reach a given Δp. For this reason, in choosing the polarimeter reaction, one first looks at analysing powers and then at the cross section of the reaction, because the the analysing power factor is more important than that from the cross section.

2.3 Spin 1

There are three possible eigenvalues of S_z with its eigenfunctions from Eq. (3). So, we have three pure state for the spin 1 particles:

$$|s=1; m=1\rangle \quad |s=1; m=0\rangle \quad |s=1; m=-1\rangle \tag{26}$$

The spin operator $\vec{S}$ is therefore a 3×3-matrix and one can write them like the Pauli operators:

$$\begin{aligned} S_x &= \frac{1}{\sqrt{2}}\begin{pmatrix} 0 & 1 & 0 \\ 1 & 0 & 1 \\ 0 & 1 & 0 \end{pmatrix} \\ S_y &= \frac{i}{\sqrt{2}}\begin{pmatrix} 0 & -1 & 0 \\ 1 & 0 & -1 \\ 0 & 1 & 0 \end{pmatrix} \\ S_z &= \begin{pmatrix} 1 & 0 & 0 \\ 0 & 0 & 0 \\ 0 & 0 & -1 \end{pmatrix} \end{aligned} \tag{27}$$

These three operators together, with 3×3 unit matrix, comprise four hermitian operators, which are linear independent. It is however evident that nine are needed to 'span' the 3×3 space. Each spin operator has to have zero trace and each will be orthogonal to the unit matrix U which means that its expectation value will be zero for an unoriented ensemble. One can construct from the available matrices:

$$S_{ij} = \frac{3}{2}(S_i S_j + S_j S_i) - 2U\delta_{ij} \qquad (\text{with } i, j = x, y, z) \tag{28}$$

With this one obtains six matrices but, since Trace(S) = 0, we get only five linear independent matrices:

$$p_{ij} = \langle S_{ij} \rangle = \mathrm{Trace}(\rho S_{ij}) \tag{29}$$

We can define p_{ij} in a same way to p_i:

$$p_{zz} = \langle S_{zz} \rangle = \mathrm{Trace}(\rho S_{zz}) \tag{30}$$

It is possible to compose a 3×3 matrix from the different components of p_{ij}, which is a second rank tensor, and defines a tensor polarization of the beam. The definition of the vector polarization is the same Eq. (27), but we can write p^*_{zz} with the occupation number of three spin states:

$$p^*_{zz} = \langle S_{zz} \rangle = \mathrm{Trace}(\rho S_{zz}) = p_+ + p_- - 2p_0 \tag{31}$$

If all three states are occupied equally in the beam, $p_+ = p_- = p_0 = 1/3$, then we have an unpolarized beam with $p^*_{zz} = 0$ and $p^*_z = 0$. In general

$$p^*_{zz} = p_+ + p_- - 2p_0 = \frac{N_+ + N_- - 2N_0}{N_{tot}} \tag{32}$$

From this it follows that:

$$-2 \leq p^*_{zz} \leq 1 \tag{33}$$

For illustration see Fig. 2. Knowing the tensor polarization gives us information about

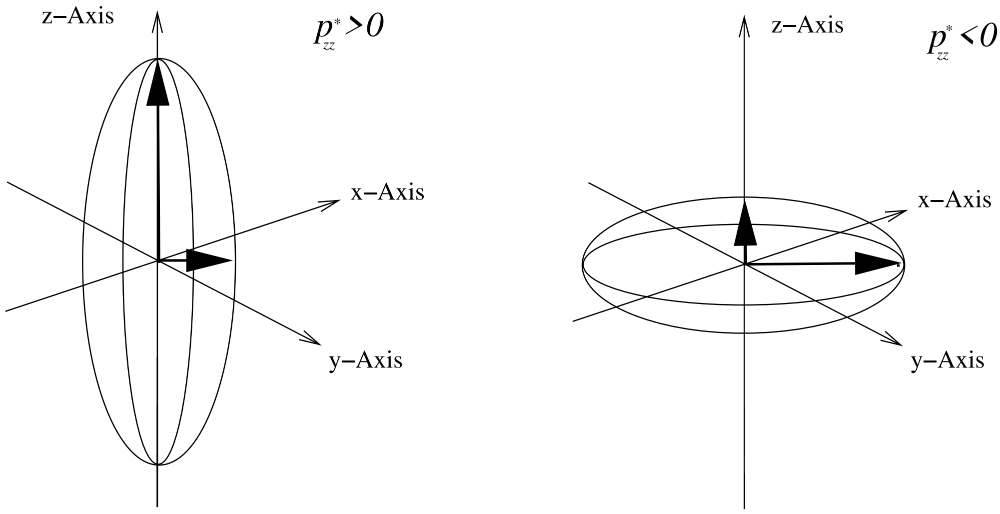

Figure 2: Positive and negative tensor polarizations

the relation between $N_+ + N_-$ and N_0. The vector polarization (relation between N_+ and N_-), together with intensity $N_{tot} = N_+ + N_- + N_0$, gives us all the information about the occupation of the states.

2.4 Measurement of tensor polarization

In the coordinate system of Fig. 1, the most general form for the cross section induced by spin-1 particles may be written:

$$\left(\frac{d\sigma}{d\Omega}\right)_{pol} = \left(\frac{d\sigma}{d\Omega}\right)_0 \left(1 + 3/2 \sum_{i=1}^{3} p_i A_i + 1/3 \sum_{i,j=1}^{3} p_{ij} A_{ij}\right) \tag{34}$$

The small p's represent the polarization of the incident beam and A's represent the analysing power of the reaction. In general, an incident beam may have all vector polarization components: p_x, p_y and p_z. Because of parity conservation, the reaction is sensitive only to the components which are normal to the scattering plane. Similarly, although an incident beam may contain all six tensor polarization components: $p_{zy}, p_{yz}, p_{xz}, p_{xx}, p_{yy}$ and p_{zz}, the reaction is sensitive, again because of parity, only to those indicated below:

$$\left(\frac{d\sigma}{d\Omega}\right)_{pol} = \left(\frac{d\sigma}{d\Omega}\right)_0 (1 + \frac{3}{2}\, p_y A_y + \frac{2}{3}\, p_{xz} A_{xz} + \frac{1}{6}\, p_{xx-yy} A_{xx-yy} + \frac{1}{2}\, p_{zz} A_{zz}) \tag{35}$$

The quantities defined are normalized so, that the vector quantities (p_x, p_y, p_z and A_y) may vary between $+1$ and -1. The tensor quantities (p_{xy}, p_{yz}, p_{xz} and A_{xz}) may vary between $+\frac{3}{2}$ and $-\frac{3}{2}$, and tensor quantities ($p_{xx}, p_{yy}, p_{zz}, A_{xx}, A_{yy}$ and A_{zz}) may vary between $+1$ and -2. The relation between spherical and Cartesian analysing powers is:

$$\begin{aligned} iT_{11} &= \frac{\sqrt{3}}{2} A_y \\ T_{20} &= \frac{1}{\sqrt{2}} A_{zz} \\ T_{21} &= -\frac{1}{\sqrt{3}} A_{xz} \\ T_{22} &= \frac{1}{2\sqrt{3}} (A_{xx} - A_{yy}) \end{aligned} \tag{36}$$

For a polarized beam produced by an ion source, in the coordinate system of Fig. 1, the polarization components are:

$$p_y = p_z^* \sin\beta \cos\phi \tag{37}$$
$$p_{xz} = -3/2\ p_{zz}^* \sin\beta \cos\beta \sin\phi \tag{38}$$
$$p_{xx-yy} = -3/2\ p_{zz}^* \sin^2\beta \cos 2\phi \tag{39}$$
$$p_{zz} = 1/2\ p_{zz}^* (3\cos^2\beta - 1) \tag{40}$$

The measured particle number in a detector is:

$$\begin{aligned} N_{(\vartheta,\beta,\phi)} = n\ N_A\ \Omega_N\ \mathcal{E}\ \sigma_0 \cdot (1 + \frac{3}{2}\ p_z^* \sin\beta\cos\phi A_y - p_{zz}^* \sin\beta\cos\beta\sin\phi A_{xz} \\ -\frac{1}{4}\ p_{zz}^* \sin^2\beta\cos 2\phi A_{xx-yy} + \frac{1}{4}\ p_{zz}^* (3\cos^2\beta - 1) A_{zz}) \end{aligned} \tag{41}$$

We can see that we have four unknown variables: p_y, p_{xz}, p_{xx-yy}, p_{zz} or p_z^*, p_{zz}^*, β , ϕ. Hence at least four detectors are necessary to determine the polarization of a spin-1 particle beam. It is not possible to calculate the polarization with the same trick as for the spin-1/2 particles, because the relations between $N_+ + N_-$ and N_0 is not sensitive to rotation of the analyzer around the beam direction by 180°. The only way left is to compare polarized and unpolarized runs. Only in some special cases is the entire description of the vector and tensor polarization of spin-1 particles is as easy as for spin-1/2 particles.

3 The beam polarization at COSY-Jülich

3.1 Ion beam polarization method

Among the various methods employed for the production of nuclear spin polarization, Stern-Gerlach separation of atoms in inhomogeneous magnetic multipole fields may be considered as the most successful. Here we will give a short introduction to the basic principles of the so-called "atomic-beam-method".

Sources of polarized protons (or deuterons) involve the preparation of neutral hydrogen atoms in such a way that the spins of the protons in the atoms preferentially point either along or opposite to an externally applied magnetic filed. The polarization of the protons is maintained when the atom is ionized, for instance by electron impact. The use of atomic hydrogen allows one to take advantage of the large magnetic moment of the electron. The electron spin j and the nucleon spin I of a ground state hydrogen atom in a zero external field couple to the total angular momentum F, with either $F = 0$ or $F = 1$. This is indicated in the familiar energy-level diagram in Fig. 3. The magnetic field is expressed in units of the critical field B_c, which corresponds to the field where the energy difference between states 1 and 3 is equal to the hyperfine splitting at zero field, $\Delta W = h \times 1420.4$ MHz. In the "weak field" region, $B \ll B_c$, electron and proton spins remain coupled and the eigenfunctions $|F, m_F\rangle$ are a suitable basis of a quantum mechanical description, with the appropriate quantum numbers F and m_F given on the left-hand side of Fig. 3. For $B \gg B_c$, electron and nucleon spins precess independently about the magnetic field direction and are no longer coupled. The eigenfunctions of the system are expressed through $|m_j, m_I\rangle$, with the appropriate quantum numbers given on the right-hand side of Fig. 3.

In the following we use arrows $(\uparrow, \downarrow)$ to indicate the electron spins and signs $(+, -)$ to denote nucleon spins. One notices from Fig. 3. that two states $|1\rangle = |\uparrow, +\rangle$ and $|3\rangle = |\downarrow, -\rangle$ exhibit a linear dependence on the external magnetic field, which indicates that these are "pure" states over the field range. The states $|2\rangle = |\uparrow, -\rangle$ and $|4\rangle = |\downarrow, +\rangle$, on the other hand, are mixed states. These can be expressed using a field-dependent mixing angle θ, given by $\tan 2\theta = B/B_c = 1/\chi$. Below in the Table 1 we give the wave functions of the four energy levels of ground state hydrogen atoms and the corresponding electron and nucleon polarizations.

The deuteron spin $I = 1$ leads to a total of six energy levels in deuterium atoms, with a ground state splitting of $\Delta W = h \cdot 327.4$ MHz. The magnetic field dependence of

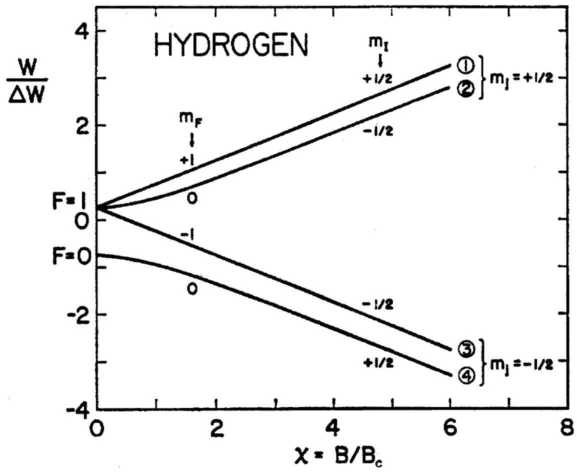

Figure 3: Breit-Rabi diagram of hydrogen atoms in units of $\Delta W = h \times 1420.4$ MHz [10]. The magnetic field is given in units of $\chi = B/B_c$. The critical field for the ground state of hydrogen is $B_c = 50.7$ mT.

	P_e	P_z
$\|1\rangle = \|\uparrow +\rangle$	$+1$	$+1$
$\|2\rangle = \cos\theta \cdot \|\uparrow -\rangle + \sin\theta \cdot \|\downarrow +\rangle$	$+\cos 2\theta$	$-\cos 2\theta$
$\|3\rangle = \|\downarrow -\rangle$	-1	-1
$\|4\rangle = \sin\theta \cdot \|\uparrow -\rangle - \cos\theta \cdot \|\downarrow +\rangle$	$-\cos 2\theta$	$+\cos 2\theta$

Table 1: Wave functions of ground state hydrogen atoms (left-hand side) and the corresponding electron and nucleon polarization (right-hand side), P_e and P_z, respectively. The mixing term is given by $\cos 2\theta = \chi/\sqrt{1+\chi^2}$, with $\chi = B/B_c$.

deuterium atoms is shown in Fig. 4. The wave functions of the six hyperfine components can be expressed in a similar way, using the mixing angles $\tan 2\theta_\pm = \sqrt{8}/(3\chi \pm 1)$, as indicated on the left-hand side of Table 2.

The production of nuclear polarization of hydrogen (or deuterium) in practice requires one to generate a population such that the four (or six) states are not equally occupied. This is accomplished by separating the atoms in a strong inhomogeneous magnetic field ($B \gg B_c$). Magnet systems consisting of sextupoles are widely used because of their harmonic focussing properties. The magnitude of the magnetic flux density inside a sextupole of inner radius r_1 and pole tip field B_0 is given by $B(r) = B_0(r/r_1)^2$. The restoring force acting on atoms with spin projection $m_j = +\frac{1}{2}$ is proportional to the gradient of the magnetic flux density, i.e. proportional to $-r$. The atoms focused therefore undergo harmonic motion in r about the beam direction, while atoms with $m_j = -\frac{1}{2}$ are deflected. In a strong magnetic field one ends up with hydrogen (or deuterium) atoms that are fully electron polarized, but possess no nuclear polarization, since all nuclear states are equally occupied. Nuclear polarization is obtained by inducing suitable radio-frequency transi-

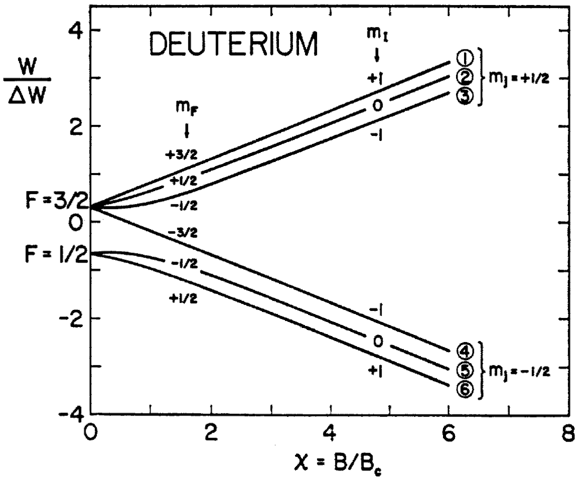

Figure 4: Energy levels of a deuterium atom in a magnetic field. The energy is measured in units of $\Delta W = h \cdot 327.4$ MHz ($= 1.4 \cdot 10^{-6}$ eV). The magnetic field is measured in units of $\chi = B/B_c = (g_j\mu_B - g_I\mu_N)B/\Delta W$. For ground state deuterium atoms $B_c = 11.7$ mT.

			P_e	P_z	P_{zz}
$\|1\rangle = \|\uparrow +\rangle$			$+1$	$+1$	$+1$
$\|2\rangle = \cos\theta_+ \|\uparrow 0\rangle$	$+$	$\sin\theta_+ \|\downarrow +\rangle$	$+\cos 2\theta_+$	$+\frac{1}{2}(1-\cos 2\theta_+)$	$-\frac{1}{2}(1+3\cos 2\theta_+)$
$\|3\rangle = \cos\theta_- \|\uparrow -\rangle$	$+$	$\sin\theta_- \|\downarrow 0\rangle$	$+\cos 2\theta_-$	$+\frac{1}{2}(1-\cos 2\theta_+)$	$-\frac{1}{2}(1+3\cos 2\theta_+)$
$\|4\rangle = \|\downarrow -\rangle$			-1	-1	$+1$
$\|5\rangle = \sin\theta_- \|\uparrow -\rangle$	$-$	$\cos\theta_- \|\downarrow 0\rangle$	$-\cos 2\theta_-$	$-\frac{1}{2}(1-\cos 2\theta_-)$	$-\frac{1}{2}(1+3\cos 2\theta_-)$
$\|6\rangle = \sin\theta_+ \|\uparrow 0\rangle$	$-$	$\cos\theta_+ \|\downarrow +\rangle$	$-\cos 2\theta_+$	$+\frac{1}{2}(1+\cos 2\theta_+)$	$-\frac{1}{2}(1-3\cos 2\theta_+)$

Table 2: Wave functions of ground state deuterium atoms (left-hand side) and the corresponding electron, nucleon vector and tensor polarization (right-hand side), P_e, P_z and P_{zz} respectively. The mixing parameter can be expressed through $\cos 2\theta_\pm = (3\chi \pm 1)/\sqrt{9\chi^2 \pm 6\chi + 9}$, where $\chi = B/B_c$.

tions.[1] However, already when atoms are moved into a weak magnetic field, the coupling of electron and nucleon spins leads to a partial transfer of the electron polarization to the nucleus. In Fig. 5 we show the field dependence of the nuclear polarization P_z of hydrogen atoms, which is given quantitatively by the expressions on the right-hand side of Table 1.

If more than one substate is populated, the polarization is given by the weighted mean using Eq. (42). In the discussion presented below, we assume equal occupation numbers if more than one state is involved, which to a good approximation is true in atomic beam applications. Thus in a weak magnetic field the two equally populated substates $|1\rangle$ and $|2\rangle$ yield a nuclear polarization of $P_z = 0.5$.

If one uses a single pure hyperfine state ($|1\rangle$ or $|3\rangle$) in a weak magnetic field, the figure

[1]Radio-frequency transitions are discussed, e.g. in refs. [11, 10]; a quantum-mechanical discussion can be found in ref. [12].

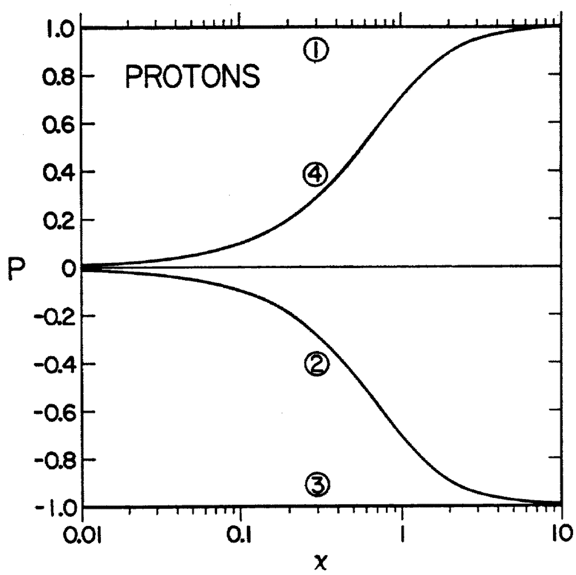

Figure 5: Magnetic field dependence of the nuclear polarization P_z of hydrogen atoms for any of the four hyperfine states shown in Fig. 3. The magnetic field is measured in units of $\chi = B/B_c$.

of merit (FOM) of the beam,

$$P_z = \frac{1}{I}\frac{\sum_m mN_m}{\sum_m N_m} \tag{42}$$

$$\text{FOM} = I \cdot P^2 \, , \tag{43}$$

where I denotes the beam intensity. The beam polarization P improves by a factor of 2 over the situation discussed above. The production of an atomic beam in a single hyperfine state ($|1\rangle$) requires *two* sextupole magnet systems and a radio-frequency transition unit placed between them. Atoms in state $|2\rangle$ are transferred by the radio-frequency transition into a state with $m_j < 0$ and are deflected in the *second* sextupole system. In addition, in that case the nuclear polarization is independent of the magnetic field, which is advantageous in certain situations. The largest figure of merit is obtained through a population of states $|1\rangle + |4\rangle$ (or $|2\rangle + |3\rangle$) in a strong field through suitable radio-frequency transitions.

The nuclear vector and tensor polarization of deuterium atoms is given by the expressions on the right-hand side of Table 2.

The vector polarization P_z varies between $+1$ and -1, while the tensor polarization P_{zz} ranges from $+1$ to -2 (see also Fig. 6).

Polarization Reversal It should be noted that the situation described above enables two different modes of operation of a polarized hydrogen or deuterium target. *(i)* The

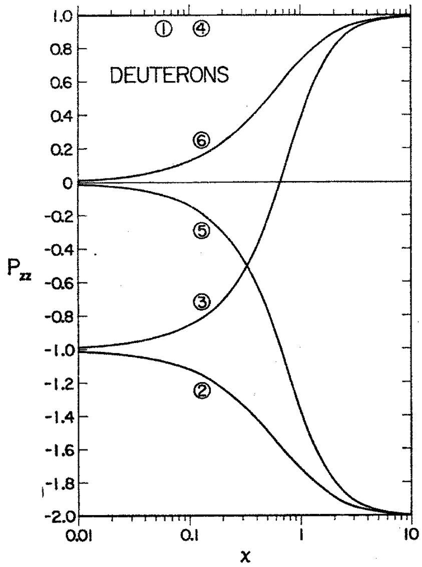

Figure 6: Magnetic field dependence of the nuclear vector and tensor polarization, P_z and P_{zz} of deuterium atoms for any of the six hyperfine states shown in Fig. 4. The magnetic field is measured in units of $\chi = B/B_c$.

reversal of the polarization of an ensemble of atoms in a weak magnetic field can be achieved simply through the reversal of a weak magnetic guide field of the order of 0.5 mT. *(ii)* The reversal of a strong field is often impractical, and it is much easier in that case to obtain polarization reversal through different combinations of hyperfine states, e.g. states $|1\rangle + |4\rangle$ for hydrogen yield $P_z = +1$, while states $|2\rangle + |3\rangle$ give $P_z = -1$.

For deuterium atoms a similar mode of operation is feasible. In a weak field a pure state of deuterium may be used, e.g. state $|1\rangle$, which gives vector polarization of $P_z = \pm 1$, depending on the orientation of the magnetic guide field. It should be noted that in this case the nuclear tensor polarization $P_{zz} = +1$ for deuterium atoms for *both* field directions. Therefore, in order to reverse the tensor polarization in a weak field, one needs radio-frequency transitions to obtain a different population of hyperfine states.

A typical scenario for deuterium atoms in a strong magnetic field is for instance an ensemble consisting of states $|1\rangle + |6\rangle$ (or $|3\rangle + |4\rangle$), which yields $P_z = +1$ (or -1) and $P_{zz} = +1$. In this case one can reverse the vector polarization, while the tensor remains constant. On the other hand it is possible, through a combination of states $|3\rangle + |6\rangle$ (or $|2\rangle + |5\rangle$), to obtain the maximum possible values for the tensor polarization $P_{zz} = +1$ (or -2) with vanishing vector polarization $P_z = 0$.

3.2 Polarized ion source

The polarized ion beam for COSY is produced in a charge exchange reaction between a ground state nuclear polarized atomic hydrogen or deuteron beam and a fast neutral cesium beam. The colliding-beams source (CBS) at COSY comprises three major components:

the atomic beam source, the Cs beam source, and the charge-exchange region (Fig. 7). The neutral, nuclear polarized atomic $\vec{\mathrm{H}}^0$ beam meets inside the charge-exchange region the fast neutral Cs^0 beam and swaps charges according to: $\vec{\mathrm{H}}^0 + \mathrm{C}s^0 \rightarrow \vec{\mathrm{H}}^- + \mathrm{C}s^+$ The negatively charged $\vec{\mathrm{H}}^-$ atoms are extracted from the charge exchange region by electric fields and are transferd to the cyclotron JULIC via a Wien-Filter to provide the proper spin alignment.

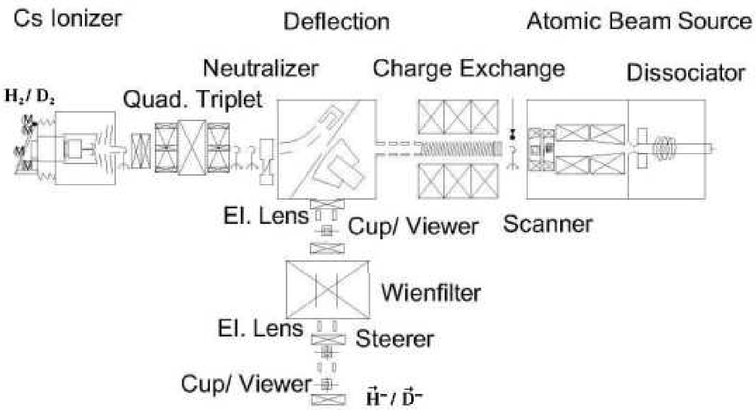

Figure 7: The COSY Colliding Beams Source

An atomic-beam source produces an intense neutral polarized atomic hydrogen beam. At first, gas molecules are dissociated in an inductively coupled 300-400 W RF-discharge. The atoms are cooled to about 30 K, while passing the aluminum nozzle of 20 mm length and 3 mm diameter. Therefore, the atoms are considerably slowed down with the conseqences that i) shorter sextupole magnets can be used, ii) the first sextupole magnet accepts an increased solid angle, and iii) the dwell time of the atoms in the charge-exchange region is increased in proportion to the decrease of the beam velocity. At the position of charge-exchange region hydrogen intensities of $I_{H^0} > 4 \cdot 10^{16}$ atoms/sec have been verified. The atomic-beam intensity could be increased substantially by a pulsing of the Cs^0 and H^0 beams.

Opposite to the atomic beam source, the fast, neutral Cs^0 beam for the charge-exchange reaction in the solenoid is produced in two steps. First, the Cs vapour is thermally ionized on a hot (1200 $^\circ$C) porous tungsten surface at an appropriate beam potential of about 40-60 kV. This beam has to be focused into the charge-exchange solenoid by magnetic quadrupoles. Usually, the charged Cs^+ beam is deflected by means of the Cs^+ deflector in front of the solenoid into a Faraday cup. Only just before the injection into the COSY ring is due, the neutralizer, placed between the quadrupoles and the solenoid, is filled with Cs vapour. As a consequence, the charged, fast fast Cs^+ beam becomes neutralized and enters the charge-exchange region inside the solenoid through an orifice in the 90 $^\circ$-deflector. The neutralizer effeciency was measured to exceed 90%.

Various H^- beam properties can be adjusted in the charge-exchange solenoid. Since the neutral polarized atomic hydrogen beam is selectively ionized by the charge-exchange process, only little background of unpolarized H^- beam is produced that could eventually impair the nuclear beam polarization. Furthermore, by varying the solenoid field, the transversal emittance can be traded for polarization.

At present, inside COSY a proton beam polarization of $P > 80\%$ and behind the injector cyclotron JULIC a polarization of $P > 85\%$ hase been measured. More than 22 μA H^- current (background < 45 nA) have been extracted from the COSY-CBS.

3.3 Acceleration of polarized protons and deuterons at COSY

The polarized H^- or D^- ion beam delivered by the source, is pre-accelerated in the cyclotron JULIC and injected by charge exchange into the COSY ring. The acceleration of vertically polarized protons and deuterons at COSY is discussed in detail for example in [14].

For an ideal planar circular accelerator with a vertical guide field, the particle spin vector precesses around the vertical axis. In this way the vertical beam polarization is preserved. The spin motion in an external electromagnetic field is governed by the Thomas–BMT equation, leading to a spin tune $\nu_{sp} = \gamma G$, which describes the number of spin precessions of the central beam per revolution in the ring. G is the anomalous magnetic moment of the particle ($G = 1.7928$ for protons, -0.1423 for deuterons), and $\gamma = E/m$ is the Lorentz factor. During the acceleration of a vertically polarized beam, depolarizing resonances are crossed if the precession frequency of the spin γG is equal to the frequency of the encountered spin–perturbing magnetic fields. In a strong–focusing synchrotron like COSY two different types of strong depolarizing resonances are excited, namely imperfection resonances caused by magnetic field errors and misalignments of the magnets, and intrinsic resonances excited by horizontal fields due to the vertical focusing. For deuterons the spin tune is about 25 times lower than for protons at the same energy. Depolarizing resonances for deuterons are therefore 25 times further apart compared to those for protons. Depolarizing resonances for deuterons are also about 13 times weaker at low energies and 25 times weaker for high energies.

In the momentum range of COSY, five imperfection resonances have to be crossed. The existing correction dipoles of COSY are utilized to overcome all imperfection resonances by exciting adiabatic spin flips without polarization losses. The number of intrinsic resonances depends on the superperiodicity of the lattice. The magnetic structure of COSY allows one to choose a superperiodicity of $P = 2$ or 6. A tune-jump system consisting of two fast quadrupoles has been developed especially to handle intrinsic resonances at COSY.

The imperfection resonances in the momentum range of COSY are listed in Table 3. They are crossed during acceleration, if the number of spin precessions per revolution of the particles in the ring is an integer ($\gamma G = k, k$ is integer). The resonance strength depends on the vertical closed orbit deviation.

A spin flip occurs at all resonances if synchrotron oscillations are not considered. However, the influence of synchrotron oscillation during resonance crossing cannot be neglected. At the first imperfection resonance, the calculated polarization with a momentum spread of $\Delta p/p = 1 \times 10^{-3}$ and a synchrotron frequency of $f_{syn} =$ Hz is about $P_f/P_i \approx -0.85$. The

γG	T_p	p	y_{co}^{rms}	ϵ_r	P_f/P_i
	GeV	GeV/c	mm	10^{-3}	
2	0.1084	0.4638	2.3	0.95	-1.00
3	0.6318	1.2587	1.8	0.61	-0.88
4	1.1551	1.8712	1.6	0.96	-1.00
5	1.6785	2.4426	1.6	0.90	-1.00
6	2.2018	2.9964	1.4	0.46	-0.58

Table 3: Resonance strength ϵ_r and the ratio of preserved polarization P_f/P_i at imperfection resonances for a typical vertical orbit deviation y_{co}^{rms}, without considering synchrotron oscillation.

resonance strength of the first imperfection resonance has to be enhanced to $\epsilon_r = 1.6 \times 10^{-3}$ to excite spin flips with polarization losses of less than 1%. At the other imperfection resonances the effect of synchrotron oscillation is smaller, due to the lower momentum spread at higher energies. Vertical correction dipoles or a partial snake could be used to preserve polarization at imperfection resonances by exciting adiabatic spin flips. Simulations indicate that an excitation of the vertical orbit with existing correction dipoles by 1 mrad is sufficient to adiabatically flip the spin at all imperfection resonances. In addition, the solenoids of the electron-cooler system inside COSY are available for use as a partial snake. They are able to rotate the spin around the longitudinal axis by about 8° at the maximum momentum of COSY. A rotation angle of less than 1° of the spin around the longitudinal axis already leads to a spin flip without polarization losses at all five imperfection resonances.

The number of intrinsic resonances depends on the superperiodicity P of the lattice, which is given by the number of identical periods in the accelerator. The COSY ring consists of two 180° arc sections connected by straight sections. The straight sections can be tuned as telescopes with 1:1 imaging, giving a 2π betatron phase advance. In this case the straight sections are optically transparent and the arcs contribute to the strength of intrinsic resonances. One then obtains for the resonance condition $\gamma G = k \times P \pm (Q_y - 2)$, where k is an integer and Q_y is the vertical betatron tune.The magnetic structure in the arcs allows adjusment of the superperiodicity to $P = 2$ or 6. The corresponding intrinsic resonances in the momentum range of COSY are listed in Table 4.

The first injection and acceleration of vertically polarized deuterons was performed in February 2003. No first-order depolarizing resonance is crossed in the momentum range of COSY at an ordinary transversal betatron tune.

3.4 The polarized COSY deuteron beam

The experiment used the polarized deuteron beam provided by the COSY ion source. As was discussed in section 2.5, after selection of electronic states $m_j = +\frac{1}{2}$, the deuteron nuclei are still not polarized since the beam contains equal population of the three deuterium magnetic substates. Usually radio-frequency transitions (RFT) are applied to induce ex-

P	γG	E_{kin} MeV	p MeV/c	ϵ_r 10^{-3}
2	$6 - Q_y$	312.4	826.9	0.26
2	$0 + Q_y$	950.7	1639.3	0.21
2,6	$8 - Q_y$	1358.8	2096.5	1.57
2	$2 + Q_y$	1997.1	2781.2	0.53
2	$10 - Q_y$	2405.2	3208.9	0.25

Table 4: Resonance strength ϵ_r of intrinsicresonances for a normalized emittance of 1π mm mrad and vertical betatron tune of $Q_y = 3.61$ for different superperiodicities P.

change between magnetic sublevels $|m_j, m_d\rangle$ in order to produce nuclear polarization. In the November 2003 run, the following set of transitions was used for the preparation of the polarized COSY deuteron beam:

RFT1 high-field single transition 361 MHz:

$$|-1/2, -1\rangle \Longleftrightarrow |-1/2, 0\rangle$$

RFT2 middle-field single transition 328 MHz:

$$|1/2, 0\rangle \Longleftrightarrow |1/2, 1\rangle$$

RFT3 weak-field triple transition 5.8 MHz:

$$\begin{aligned} |3/2, 1\rangle &\Longleftrightarrow |-3/2, -1\rangle \\ |1/2, 0\rangle &\Longleftrightarrow |-1/2, -1\rangle \\ |-1/2, 0\rangle &\Longleftrightarrow |1/2, 1\rangle \end{aligned}$$

The scheme consists of eight different polarization states, including one unpolarized mixture and seven combinations of vector and tensor polarizations, as shown in Table 5.

For each injection into COSY, the polarized ion source was switched to a different polarization state. The duration of a cycle was sufficiently long (200 sec) to ensure stable conditions for the injection of the next state. After the seventh state, the source was reset to the zeroth mode and the pattern repeated. The ANKE data acquisition system received status bits from the source, latched during injection, that ensured the correct identification of the polarization states during the experiment. Because of their small magnetic moment, deuterons encounter no depolarising resonances in the energy range of COSY and are therefore unlikely to be depolarized. This was recently tested for a vector polarized beam, at least qualitatively, during the SPIN@COSY experiment [13]. It should be noted, that the present experiment is the first one that provides at one and the same time a measurement of both vector and tensor polarizations of the deuteron beam stored in COSY.

This set of transition allows 8 basic combinations which are summarized in Table 5, together with the corresponding maximum values for P_z and P_{zz}

Spin Mode	Vector P_z max	Tensor P_{zz} max	Pattern	Intensity $[I_0]$	1st 6pole	RFT1	2nd 6pole	RFT2	RFT3	m_I
0	0	0	000	1	123	123	123	123	123	+1, 0, -1
1	-2/3	0	001	1	123	123	123	123	432	-1, -1, 0
2	+1/3	+1	010	1	123	123	123	163	163	+1, +1, -1
3	-1/3	-1	011	1	123	123	123	163	452	-1, 0, 0
4	+1/2	-1/2	100	2/3	123	125	12	12	12	+1, 0
5	-1	+1	101	2/3	123	125	12	12	43	-1, -1
6	1	+1	110	2/3	123	125	12	16	16	+1, +1
7	-1/2	-1/2	111	2/3	123	125	12	16	45	-1, 0

Table 5: Modes of the polarized deuteron ion source. The intensity modulations between the different modes constitute a compromise in order to achieve higher polarizations. I_0 refers to the maximum number of deuterons delivered by the source and stored in COSY. In our experiment an intensity of about $I_0 = 3 \times 10^9$ was achieved.

4 Experimental Set-up

The experiments have been performed at the magnetic spectrometer ANKE at the COoler SYnchrotron COSY. For the Charge-Exchange deuteron breakup study the ANKE forward detection system and the silicon telescope (spectator detector) were used. The ANKE forward system allows the detection of particles emitted at small angles and high momenta. The silicon telescope was used for the selection of *pp* quasi-free reaction with the aim of determining the beam polarization and cross-check the luminosity. In this chapter a technical overview of the detector system is given.

4.1 The COSY accelerator

The COoler SYnchrotron COSY-Jülich [15] provides high precision ($\Delta p/p = 10^{-4} - 10^{-3}$) unpolarized and polarized proton and deuteron beams in the momentum range from 300 MeV/c up to 3.7 GeV/c. An electron cooling system reaches up to a momentum of 600 MeV/c and is complemented by a stochastic cooling that covers the upper range from 1.5 to 3.7 GeV/c. In Fig. 8 the layout of COSY is shown. Polarized beams are produced at COSY using a polarized ion source originally developed by a collaboration of the universities of Bonn, Erlangen, and Cologne [16]. The source provides a vector polarized proton beam and all possible combinations of vector and tensor polarized deuteron beams. In a strong focusing synchrotron like COSY, imperfection and intrinsic resonances cause polarization losses during acceleration (see section 2.7). The existing magnet system of COSY allows one to overcome all imperfection resonances by exciting adiabatic spin flips without polarization losses. A tune-jump system consisting of two fast quadrupoles (Fig. 8) has been developed to handle intrinsic resonances in COSY. This magnetic system is being successfully utilized at all intrinsic resonances in the momentum range of COSY. The main diagnostic tool to develop polarized beams in COSY is the EDDA detector [3]. The polarization is determined at EDDA by measuring the asymmetry of scattering of the circulating COSY beam on carbon or CH_2–fibre targets. Additional polarimeters are installed in the injection beamline to COSY, in the COSY ring, and in the extraction beamline of COSY (Fig. 8). The intensity of the polarized beam in COSY can be increased by stacking injection with an electron–cooler and the beam quality can be further improved with stochastic cooling systems [17, 18]. COSY beams are being delivered to four internal (ANKE, COSY–11, EDDA, PISA) and five external experiments (TOF, MOMO, GEM, NESSY and JESSICA).

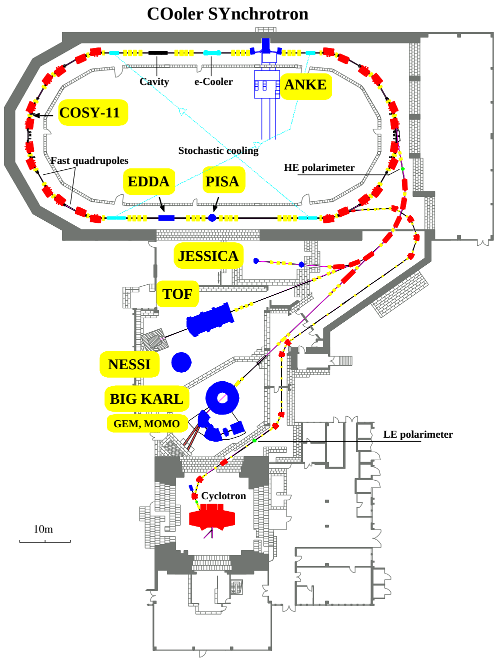

Figure 8: The COoler SYnchrotron COSY at the Forschungszentrum Jülich.

4.2 The ANKE spectrometer

The experiment was performed at the ANKE spectrometer [19] ("Apparatus for studies of Nucleon and Kaon Ejectiles") installed at the internal beam of COSY. In Fig. 9 the ANKE spectrometer is shown. The main components of the spetrometer are: a magnetic system, an internal target and four detection systems: positive and negative side detectors, forward and backward detectors. The ANKE magnetic system consists of a dipole magnet D1 which deflects the circulating COSY beam by an angle α, a large spectrometer dipole magnet D2 (beam deflection -2α), and a third dipole magnet D3, identical to D1, to

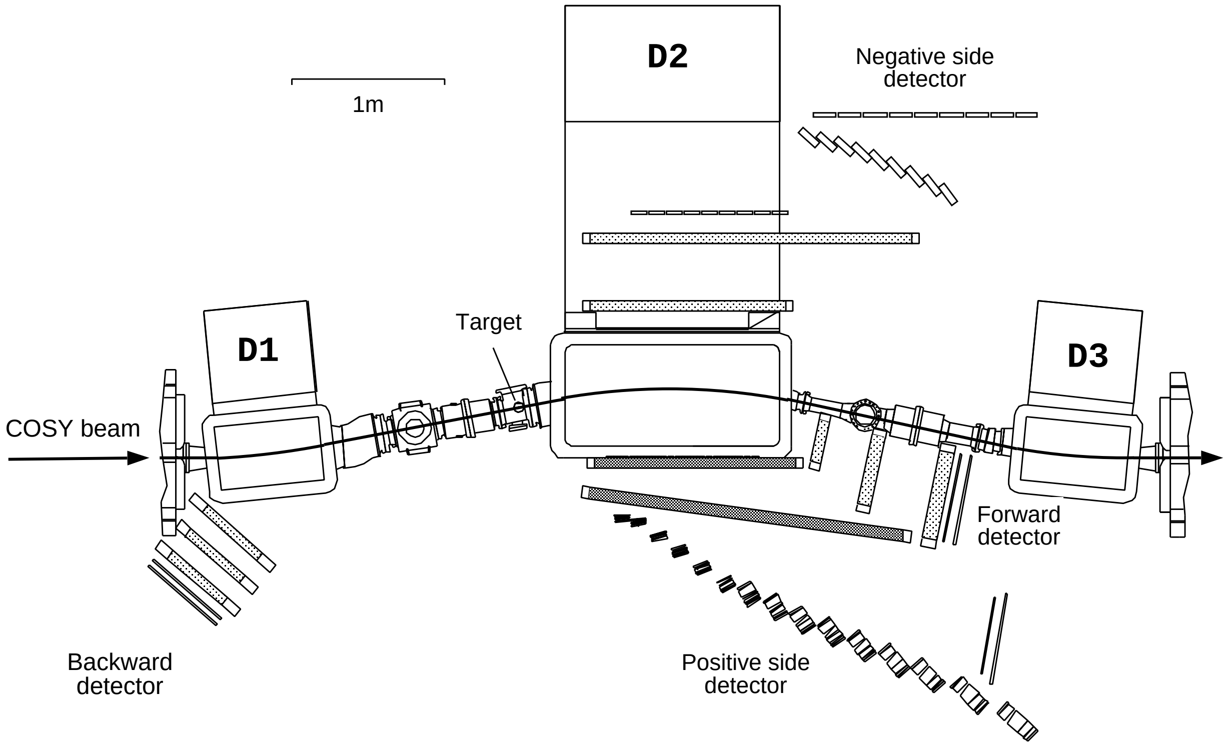

Figure 9: Schematic drawing of ANKE Spectrometer

deflect the beam by α back to the nominal orbit. The deflection angle of the beam can be adjusted to optimize the magnetic field up to 1.56 T independent of the COSY beam momentum. There are two types of targets available at ANKE: a strip target (carbon, polyethylene or any other solid material) and a cluster beam target [20], producing a beam of hydrogen or deuterium clusters that cross the COSY beam. A frozen pellet target for high luminosity measurements [21] and a polarized storage-cell gas target [22], fed by an atomic beam source (ABS) for polarization measurements are also being developed. The momentum acceptance of the positive and negative side detectors is in the range of about 0.3 to 0.8 GeV/c. The forward detector, allowing one to detect positively charged particles in momentum range 0.3–3.7 GeV/c, is used in a number of experiments at ANKE, e.g. the a^0 production study [23], the ω, η production on effective neutron target [24, 25], the deuteron breakup study [26], charge exchange breakup [8], etc. The polarized deuterons stored in the COSY ring ($\approx 3 \times 10^9$ deuterons) impinge on a hydrogen cluster–jet target (thickness $\approx 1 \times 10^{14}$ atoms/cm^2, resulting in a luminosity of $\approx 3 \times 10^{29}$ cm^{-2}s^{-1}).

4.3 The forward detector system

In Fig. 10 those parts of the spectrometer are shown that are relevant for the present experiment.

The forward detector is located between the spectrometer dipole D2 and the dipole D3,

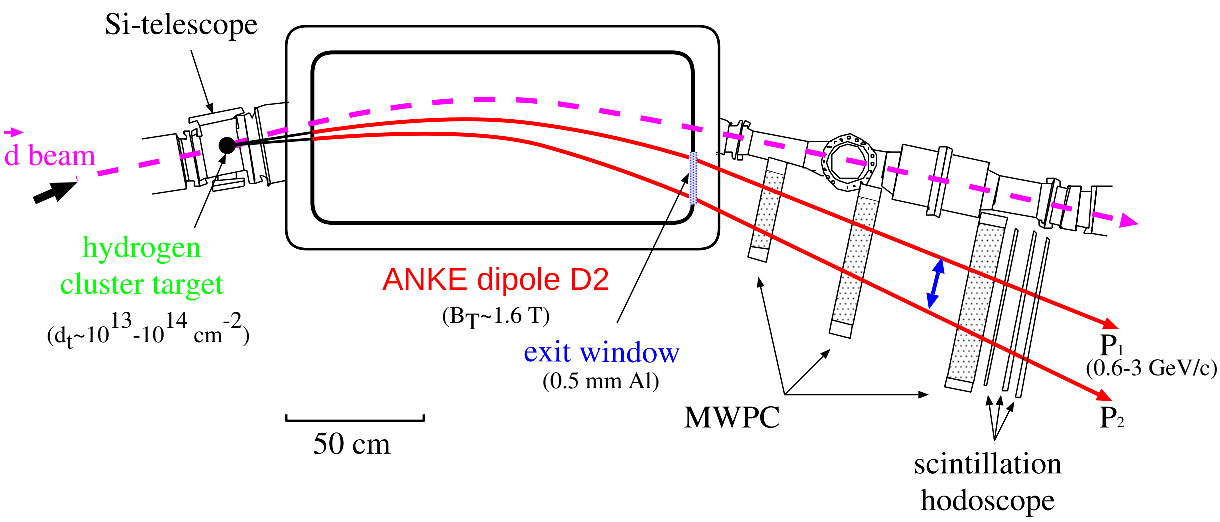

Figure 10: Schematic drawing of the part of ANKE used in the $\vec{d}p \to (pp) + n$ experiment

though the available space is rather limited there. The gap between the dipoles is 1.6 m in length and the distance between the accelerator beam tube and the ANKE side detector is about 0.7 m. Such a location results in severe requirements on the tracking system. Due to closeness to the beam pipe, it must be able to operate at rather high counting rates ($> 10^5\text{s}^{-1}$). In addition, because of the short distance between the MWPCs, one has to achieve high spatial resolution (better than 1 mm). Such spatial resolution leads to a momentum resolution of about 1%, which allows one to distinguish proton pairs with small excitation energy $E_{pp} < 3$ MeV. Particles emitted at small angles and high momenta pass the detector region close to the beam pipe, which means that the width of the chamber frame must be minimized on the side of the beam pipe.

The FD system comprises three MWPCs in total. Each of them is composed of one X and one Y module. Every module contains a wire and a strip plane. In what follows, the planes located in an $X(Y)$ module will be referred to as the $X(Y)$. Wires are oriented vertically in the X wire planes, and horizontally in the Y planes. The strips are inclined by 18° with respect to the vertical axis in the X planes, and by −18° in the Y planes. The MWPCs are mounted on a common support frame with the forward hodoscope.

The hodoscope consists ot two layers, containing 8 and 9 vertically oriented scintillators (4 to 8 cm width, 1.5 to 2 cm thickness). The timing and amplitude signals are read out via photomultipliers placed on both ends of each scintillator. It provides a trigger signal, an energy loss measurement, and allows for the determination of the differences in arrival times for particle pairs hitting different counters. Off-line processing of the amplitude data permitted the measurement of the energy-loss with 10% accuracy, and of the time-of-flight difference of events with two registered particles with a precision of 0.5 ns (rms).

The chambers produce signals 6 ns long (FWHM) for the wire planes and 30 ns long for the strip ones. The time jitter of the signals is small, being around 8 ns for the wire pulses. This allows effective operation with short strobe signals. At the set-up, the time resolution

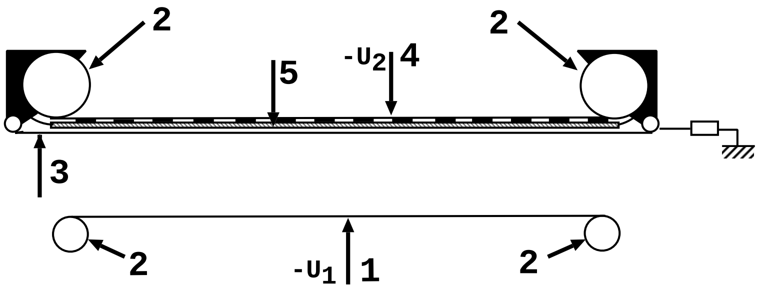

Figure 11: Schematic layout of a MWPC module. 1 — drift electrode; 2 — support rods; 3 — anode wires; 4 — mylar cathode foil with strips; 5 — high resistance foil.

of the tracking system is limited by the read-out electronics [42], which needs strobes more than 50 ns wide (while the chambers themselves could work with much shorter strobe pulses). The average number of wires fired by a crossing particle (cluster width) is close to unity, which leads to a high precision of coordinate measurements.

4.4 Acceptance of the forward detection system

The horizontal acceptance of the set–up for $T_d = 1.2$ GeV is shown in Fig. 12, whereas the vertical acceptance corresponds to $\pm 3.5°$. Deuterons from dp elastic scattering falling within the ANKE acceptance are also indicated. These events will be used for both luminosity determination and detector calibration. Also shown are pions and tritons from the $dp \to t\pi^+$ reaction and ^{3}He from the isospin–related $dp \to {}^3\mathrm{He}\,\pi^0$ reaction. Since the tensor Analysing power T_{20} has been well measured for both forward and backward pion production as a function of energy [33] (see Fig. 18), these two reactions can be used as the basis for a polarimeter for the deuteron beam.

A measurement of T_{22} requires us to detect scattering angles away from zero degrees, where this observable vanishes. Making use of the transverse positioning capability of the D2 magnet, the angle interval accepted in the forward detector can be optimized for this purpose.

4.5 Silicon-detector telescope

A silicon-detector telescope system, consisting of three layers of silicon strip detectors [30], is mounted in the target vacuum chamber as a near-target detector. To achieve tracking, energy determination and particle identification within the boundary conditions of restrected space inside the vacuum chamber of ANKE, a telescope structure of three layers of silicon detectors has was chosen. For particle identification via the $\Delta E/E$-method, the particle has to be stopped after traversing a preceding detector and depositing part of its energy in it. The ANKE silicon telescope [31] was developed to study reactions with an effective neutron target [32]. The main task for this detector is the identification of a low-energy spectator protons in pd, dp or dd collisions, down to a proton kinetic energy

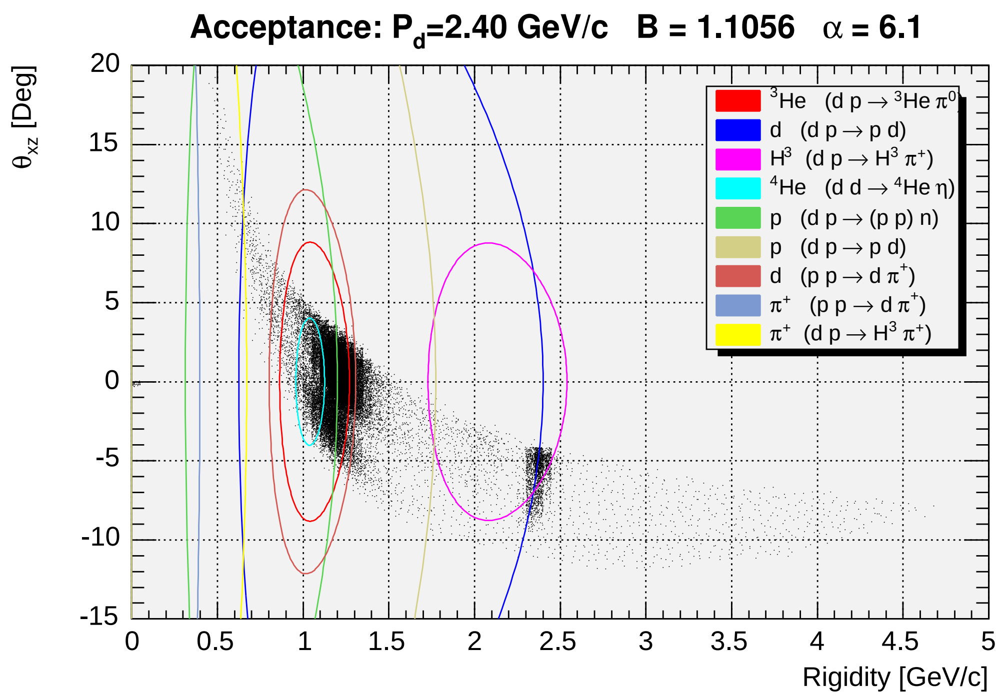

Figure 12: MC simulation of the ANKE acceptance, showing angle *versus* rigidity (p/Z). θ_{xz} is the scattering angle of the emitted particle projected onto the median plane of the spectrometer. The curves show kinematic loci of different processes.

of 2 MeV. In addition, the very clean separation of deuterons from dp elastic scattering provides the possibility to measure the absolute luminosity and to determine the beam vector polarization.

4.6 Data taking in November 2003

As a first step, during this short test measurement we aimed to take data with the vertically polarized deuteron beam on the unpolarized cluster target. Data were collected for a total of about 60 hours of measurement.

The main trigger (Tr1) for the experiment was a single-particle trigger, generated by a particle hiting a counter in the first FD hodoscope plane and one of the two counters behind in the second plane. This trigger, selecting mainly single protons, was used with a prescaling factor 10. In parallel the trigger from the silicon-detector telescope alone has been used (Tr2), in order to have the possibility of identifying quasi-elastic pp scattering for the deuteron vector polarization measurements. A special trigger (Tr3), based on energy loss in the forward hodoscope, was used to identify ^{3}He particles to select events from the polarimetry reaction $\vec{d}p \to {}^3\mathrm{He}\,\pi^0$. A scaler trigger (Tr4) was used to read out the scalers periodically ten times per second. For each trigger signal (except Tr4), all subsystems of ANKE were read out. This includes the full forward system and the silicon telescope.

The Beam Current signal (BCT) was fed into a voltage–to–frequency converter at the EDDA electronics, transformed into an optical signal to avoid signal deterioration and sent over to ANKE, where it was fed, after conversion back to a NIM–signal, into the ANKE scaler system. In this way the BCT signal becomes available in the normal ANKE data stream.

As one example of the experimental conditions, the ratio of L/BCT is shown in Fig. 13 for the spin-mode zero (unpolarized beam), where L denotes the luminosity, determined in this experiment with an accuracy $< 10\%$ (see the next section) and BCT signal, known to about 1%. This ratio contains the information about the target behaviour run by run.

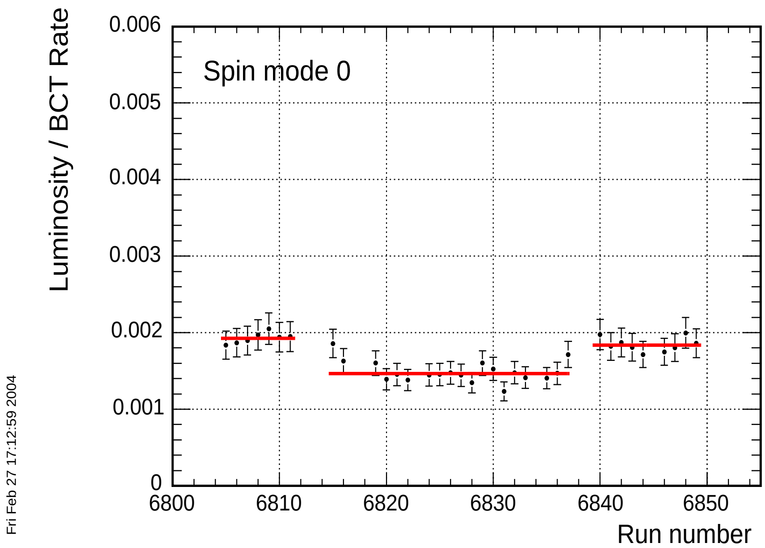

Figure 13: Target 'oscillation' run by run.

5 Luminosity

5.1 Normalization concept

The absolute normalisation of the cross-section with an accuracy of about 5% requires accurate data from a known reaction falling within the detector acceptance.

The luminosity for all the runs was evaluated using *dp* elastic scattering with a single deuteron registered in the Forward Detector at the small scattering angles in the laboratory system of 4° to 10° (see Fig. 12). Because this process has a large cross section and is not suppressed much by the acceptance of set-up, it is very clear in the momentum and angle–momentum spectra, and is thus easily selected.

The *dp* total, inelastic, and elastic total and differential cross sections have been measured at 10 momenta in the range $2.0-3.7$ GeV/c [34]. The slope parameters of the forward portions of the differential cross sections were measured to about 5% at all momenta.

From fits to these data we found a function to describe the differential cross section at $p_d = 2.40$ GeV/c in our angular interval. This is shown as the red line in Fig. 14, together with experimental data [34] at $p_d = 2.46$ GeV/c. The error entering the luminosity determination was estimated to be about $\approx 8\%$ (see solid blue line corridor).

To check the value of the luminosity obtained with the dp elastic process, we will attempt to obtain the same value from quasi-free pp scattering, using information extracted from the telescope system in concidence with the forward detector. These data are not yet available.

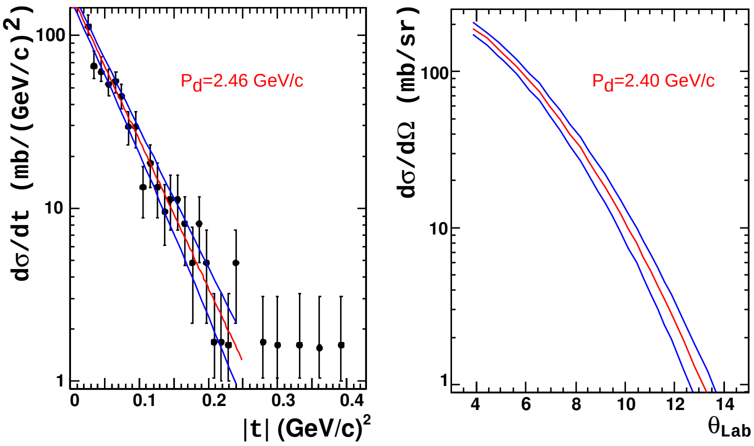

Figure 14: The invariant elastic $dp \rightarrow dp$differential cross section at p_d=2.46 GeV/c from experiment [34] (left panel). The lab differential cross section recalculated from these data at p_d=2.40 GeV/c is shown in the right panel as a red line.

5.2 Luminosity determination by *dp* elastic process

Deuterons from the spin-zero mode events (unpolarized beam) were analyzed in one degree bins in polar angle intervals in the range $4^\circ - 10^\circ$. The acceptance was calculated using a GEANT-based simulation program that includes a realistic description of the set-up. In view of the dependence of acceptance on θ_{lab}, we concentrated on the region of $\theta_{lab} = 5.5^\circ - 9^\circ$, where the acceptance changes smoothly.

The elastic peak region in the momentum spectrum of the single track events (see left panel of Fig. 15) was fitted by the sum of a Gaussian and linear function, and events were selected within 3σ from the fitted average momentum value. In the right panel of Fig. 15 an example of such a fit is shown.

After correction of the counts for the dead-time and acceptance, the luminosity of the different polar angle bins was calculated. The weak dependence of the luminosity on polar angle is shown in Fig. 16. By averaging the luminosity over the polar angle, mean values are obtained. The errors correspond to a root mean squared deviations of the luminosities,

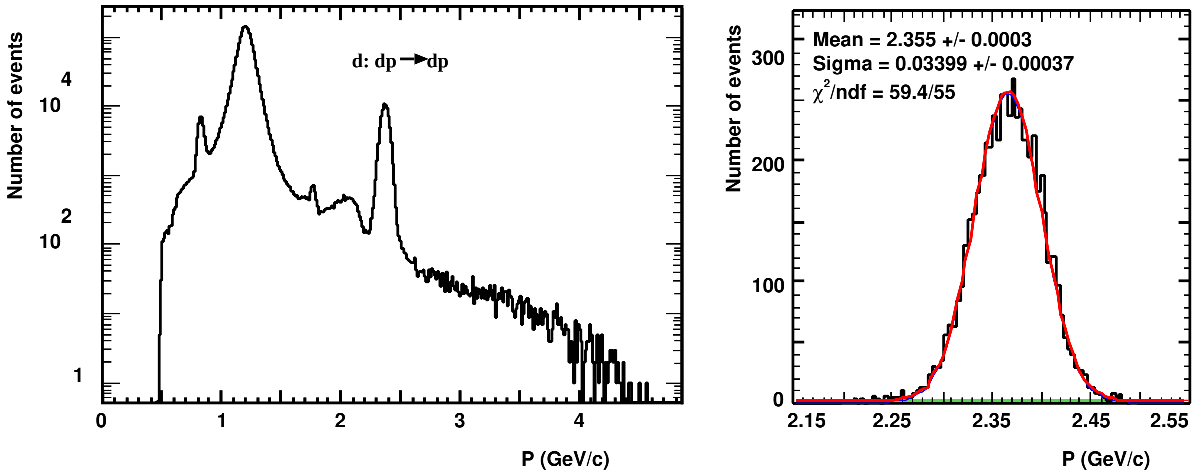

Figure 15: Left panel: Single-track momentum spectrum for the *dp* data with a deuteron beam of 2.40 GeV/c. Right panel: Fit result of the elastic peak region with the sum of a Gaussian and linear function.

determined for individual angular bins. These errors were considered as one source of systematic uncertainties.

In parallel to the charge-exchange break-up and *dp* elastic scattering, we detect quasi-free *pp* scattering using the silicon telescope system placed close to the target region in coincidence with the Forward Detection system. This reaction, which will eventually be used for the measurement of the vector polarization component of the deuteron beam, can also be considered as an additional reaction for checking the cross section normalization.

5.3 Acceptance calculations

The FD acceptance was calculated using a GEANT–based simulation program that includes a realistic description of the D2 dipole and the FD. Events with *dp* elastic kinematics were generated in a polar angle interval of forward emitted deuteron ranging from $\theta_{lab} = 0^{\circ} - 20^{\circ}$ and the azimuth ϕ was randomly distributed in the range of $0 - 180^{circ}$. The criteria for accepting an event during the simulation were:

- Particles emitted do not hit constructional elements of D2, particularly the poles of the magnet.

- Particles exit through the forward window of D2.

- Particles cross the sensitive region of the forward MWPCs, that is, the number of wires hit calculated from the track intercept is in the valid range.

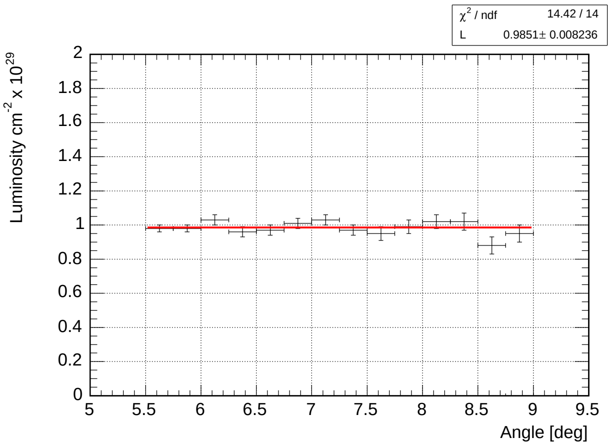

Figure 16: Angular dependence of the luminosity determined for dp forward scattering for single run. The error bars are purely statistical.

- Particles cross the first and second planes of the FD hodoscope, which corresponds to the hardware trigger condition.

As a result we obtained the dependence of the acceptance on the polar angle shown in Fig. 17.

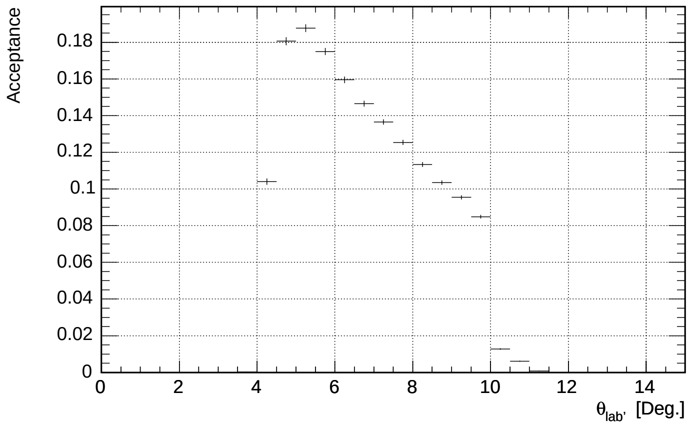

Figure 17: FD acceptance for dp elastic scattering in the full angular range.

6 Polarimetry

6.1 Analysing power of the polarimetry reactions

The deuteron vector polarization can be measured by Analysing the azimuthal asymmetry of the fast protons from the quasi–free proton scattering on the hydrogen target. For an unpolarized target, the analysing power of $\vec{d}p \to (pn)p$ quasi–free process is known from the measurements of pp elastic scattering [35], which can be identified well using the

ANKE spectator detector (silicon telescope). A similar method was already used at JINR Dubna [36] and at Saturne [37].

The tensor analysing power T_{20} for the $\vec{d}p \to {}^3\mathrm{He}\,\pi^0$ channel was measured in the forward and backward c.m. directions at 19 energies between 0.5 and 2.2 GeV at Saturne [33]. The measured value of the T_{20} which we are using in the P_{zz} estimation for our beam energy (T_d=1.2 GeV), was determined in [33] with a good accuracy ($\sim 2\%$):

$$T_{20} = -0.661 \pm 0.0157\,.$$

The energy dependence of the T_{20} measurement from these data is shown in Fig. 18.

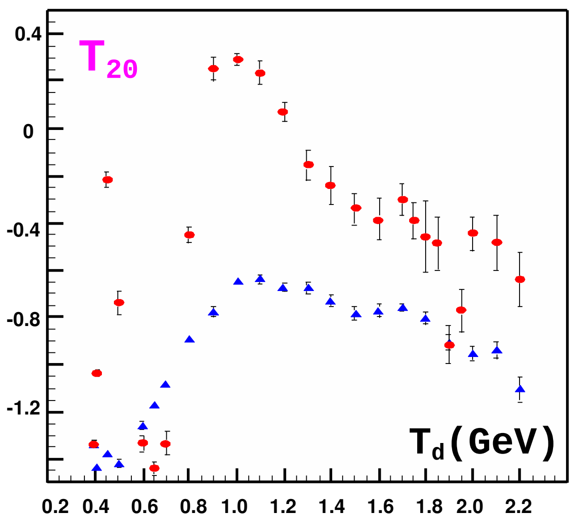

Figure 18: Saturne data on the T_{20} measurement for the reaction $\vec{d}p \to {}^3\mathrm{He}\,\pi^0$ [33]

Furthermore, the angular distributions of the vector (A_y) and tensor (A_{yy}) analysing powers of $\vec{d}p$ elastic scattering were measured at SATURNE at 1.2 GeV, in the range ($\theta_{cm} = 32^\circ - 180^\circ$) [38].

The values of the A_y and A_{yy} that we are using in the P_z estimation were also well measured in [38] over our angular range:

$$\begin{aligned} A_y(9.5^\circ_{Lab}) &= 0.427 \pm 0.013 \\ A_{yy}(9.5^\circ_{Lab}) &= 0.647 \pm 0.029\,. \end{aligned}$$

These two reactions have large enough cross sections to be detected with good statistical accuracy and used for the polarimetry.

A third reaction that can be used for the same reason is the Charge-Exchange deuteron breakup $\vec{d}p \to (2p)n$. As an analysing power (T_{20}) for this reaction we can use the prediction of the undistorted Bugg & Wilkin model, which descibes well data published at lower and higher energies [7]. For our energy we used the value of $T_{20} = 0.42$, which is predicted with an accuracy of better than 5%.

6.2 Identification of the polarimetry reactions

In the reaction $dp \to {}^3\mathrm{He}\,\pi^0$ two particles are produced, one neutral and one of charge two and so the π^0 is identified through the missing mass using only the ^{3}He information. The result for the isolation of this reaction is shown in Fig. 19. The high momentum branch of ^{3}He particles was identified well by off-line analysis applying two-dimensional cuts in ΔE *versus* momentum and Δt *versus* momentum for individual layers of the forward hodoscope (an additional layer of the sidewall hodoscope was used behind the forward hodoscope). Though the peak in Fig. 19 is wide, this is not critical since, apart from the radiative capture, there is no physical background over this region.

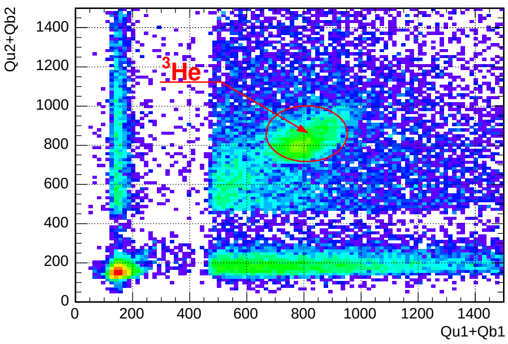

(a) ^{3}He identification

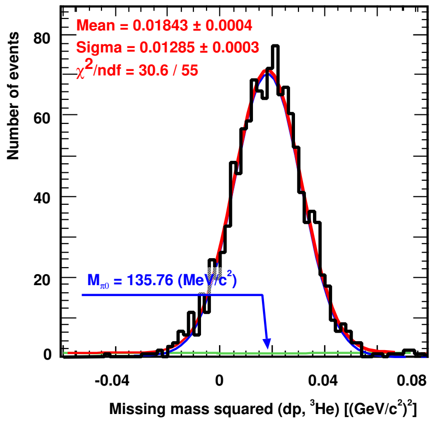

(b) Missing mass squared for the reaction $dp \to {}^3\mathrm{He}\,X$. The result of the peak fit is indicated.

Figure 19: Identification of the $dp \to {}^3\mathrm{He}\,\pi^0$ reaction.

The first step in processing the dp Charge-Exchange breakup data is to choose two-track events using the MWPC information. The momentum vectors were determined employing the magnetic field map of the spectrometer on the assumption of a point-like source placed in the centre of a beam-target interaction region. Fig. 20a displays double-particle events on a scatter plot of the particle momenta p_1 *vs* p_2. The smallness of the FD solid angle acceptance leads to a kinematical correlation for events with two or three particles in the final state (Fermi motion slightly disperses the correlation for the corresponding quasi-free processes). No assumption on the masses of the particles is required for such a correlation. The break-up events clearly manifest themselves among several processes recorded in the spectrometer. For the events with particles hitting different counters in the hodoscope, the correlation of a measured time difference Δt_{meas} with a difference of the time of flight Δt_{tof} may be observed. The time of flight from the target to the hodoscope is calculated in accordance with a measured momentum and the assumption of the proton mass for the particle. Real proton pair events are located then at the diagonal of the scatter plot (Fig. 20b).

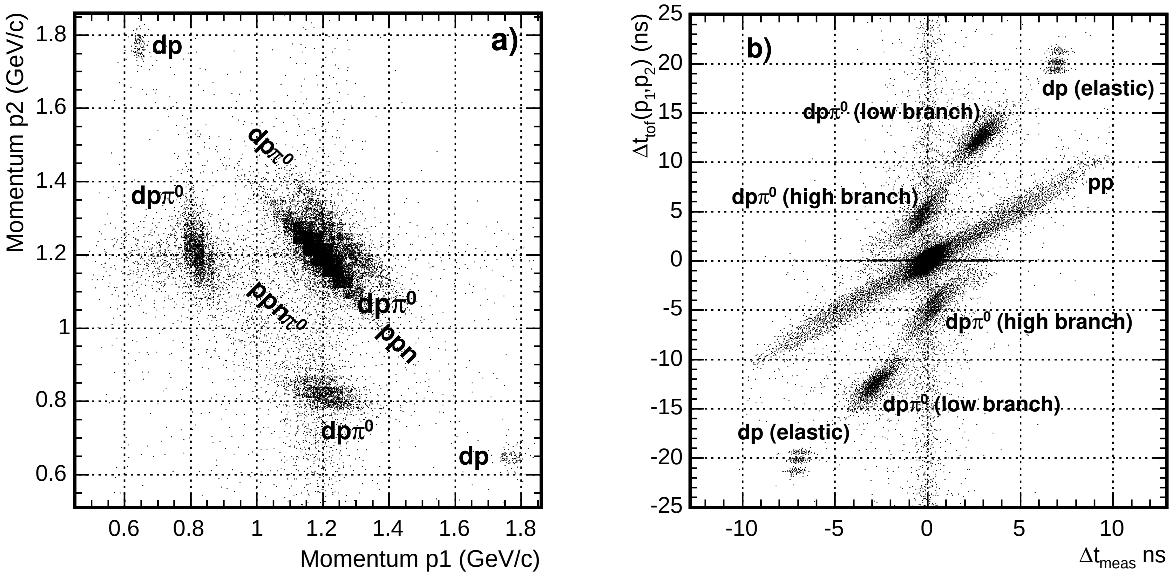

Figure 20: Identification of the particle pairs: a) Momentum correlation; b) Correlation of the time-differences

The charge-exchange process was identified from the missing-mass with respect to the observed proton pairs (see Fig. 21) and time difference information. The spectra for all spin modes reveal a well defined peak at M_{miss} equal to the neutron mass to within 1%; the mean value for the reconstructed neutron mass is $M_n = 940.4 \pm 0.2$ MeV/c^2. The background was less than 2% and stable, so that the charge-exchange process was identified with high accuracy.

Therefore, using the processes $\vec{d}p \to {}^3\text{He}\,\pi^0$ and $\vec{d}p \to (2p)n$ (for the P_{zz} measurement), $\vec{d}p \to dp$ (for the P_z and P_{zz} measurement), and quasi-free $\vec{p}p$ scattering (for the cross checking of P_z measurement), a simultaneous calibration of the vector and tensor components of polarized deuteron beam at COSY becomes possible for the first time.

6.3 P_{zz} measurement using the reaction $\vec{d}p \to {}^3\text{He}\,\pi^0$

The differential cross section for the polarized deuteron beam can be expressed in the following form [9]:

$$\frac{d\sigma^{\uparrow}}{d\Omega}(\vartheta,\varphi) = \frac{d\sigma_{\circ}}{d\Omega}(\vartheta)\left\{1 + \frac{3}{2}P_z A_y(\vartheta)\cos\varphi + \frac{1}{4}P_{zz}[A_{yy}(\vartheta)(1+\cos 2\varphi) + A_{xx}(\vartheta)(1-\cos 2\varphi)]\right\}$$

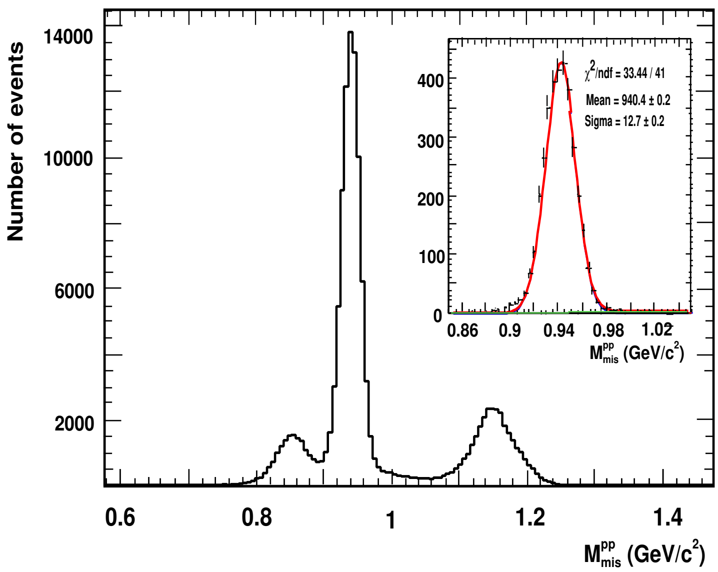

Figure 21: Missing mass distribution of all observed proton pairs. The inset shows the distribution near the neutron mass for the pairs selected by the time-of-flight difference.

For the case of $\vartheta \approx 0°$, we get:

$$\frac{d\sigma^{\uparrow}}{d\Omega}(\vartheta,\varphi) = \frac{d\sigma_{\circ}}{d\Omega}(\vartheta)\ \left\{1 + \tfrac{1}{2}P_{zz}A_{yy}(\vartheta)\right\}\ ,$$

where, for $\vartheta = 0°$, $A_{yy} = -T_{20}/\sqrt{2}$. Finally the deuteron beam tensor polarization (P_{zz}) is obtained from the known tensor analysing power (T_{20}) as:

$$P_{zz} = \frac{2\sqrt{2}}{T_{20}}\ \left[\frac{d\sigma_{\circ}}{d\Omega}(\vartheta) - \frac{d\sigma^{\uparrow}}{d\Omega}(\vartheta)\right] \Big/ \frac{d\sigma_{\circ}}{d\Omega}(\vartheta)\ .$$

For each of the spin modes of the COSY beam we identify the polarimetry reaction run by run using the missing-mass technique. The mean value for the reconstructed pion mass was close to $M_{\pi^0} = 135.4 \pm 3$ MeV/c^2 for all runs. The background was less than 4% and stable. After the correction of the counts in a $\pm 2.5\,\sigma$ range of missing mass (around 150-200 events for each spin mode in a $1°$ interval of the ^{3}He particles) on the dead-time (which is different for each spin mode) and normalizing them on the BCT signals, we calculate the P_{zz} value assuming that we are selecting polarimetry reaction at zero degrees and that $P_z \approx 0$. The results for the P_{zz} measurement for each run are shown in Fig. 22 and the average values for each spin mode in Table 6. The error burs are statistical.

6.4 P_{zz} measurement using the reaction $\vec{d}p \to (2p)n$

Using the predicted value of T_{20} [7] for the Charge-Exchange deuteron breakup $\vec{d}p \to (2p)n$ reaction, we determine the P_{zz} value run by run using the same formalism as it was applied for the $\vec{d}p \to {}^3\text{He}\,\pi^0$ process. The break-up events were selected with small excitation energy ($E_{pp} < 2$ MeV) in the near zero degree polar angle cone for the forward going proton pair for each spin mode. Then, comparing unpolarized and polarized counts, we determine P_{zz} component of the deuteron beam, which is shown in Fig. 23 and presented in table 6.

6.5 P_z measurement using the reaction $\vec{d}p \to dp$

Based on the known form of the differential cross section [9], and assuming that the ANKE acceptance of the azimuthal angle is around 180°, which means that $\cos 2\varphi \approx 1$ and $\cos\varphi \approx -1$, we obtain the following expression for P_z:

$$P_z = \frac{2(\frac{d\sigma^{\uparrow}}{d\Omega}(\vartheta) - \frac{d\sigma_{\circ}}{d\Omega}(\vartheta)) - \frac{d\sigma_{\circ}}{d\Omega}(\vartheta) P_{zz} A_{yy}}{3\frac{d\sigma_{\circ}}{d\Omega}(\vartheta) A_y < \cos\varphi >},$$

where the values of A_y and A_{yy} are known [38].

The results of the P_z measurement for each run with the same method used for P_{zz} measurements are shown in Fig. 24 with the averaged values per source state being given in Table 7.

Spin Mode	P_{zz} (${}^3\text{He}\,\pi^0$)	P_{zz} (ppn)	P_{zz} (EDDA)	P_{zz} (ideal)
1	-0.041 ± 0.096	-0.032 ± 0.048	0.057 ± 0.051	0.000
2	0.465 ± 0.106	0.520 ± 0.046	0.594 ± 0.050	1.000
3	-0.678 ± 0.087	-0.422 ± 0.052	-0.634 ± 0.051	-1.000
4	-0.099 ± 0.113	-0.204 ± 0.059	-0.282 ± 0.052	-0.500
5	0.649 ± 0.125	0.526 ± 0.053	0.537 ± 0.052	1.000
6	0.701 ± 0.128	0.576 ± 0.054	0.545 ± 0.050	1.000
7	-0.292 ± 0.108	-0.250 ± 0.058	-0.404 ± 0.053	-0.500

Table 6: Average values of P_{zz} obtained from the EDDA measurements prior to our experiment at lower energies and intensities compared with the values obtained from our $\vec{d}p \to (pp)n$ and $\vec{d}p \to {}^3\text{He}\,\pi^0$ measurements.

Spin Mode	P_z (P_{zz} from $^3\mathrm{He}\,\pi^0$)	P_z (P_{zz} from ppn)	P_z (P_{zz} from EDDA)	P_z (ideal)
1	-0.540 ± 0.023	-0.533 ± 0.022	-0.499 ± 0.021	-0.667
2	0.177 ± 0.021	0.206 ± 0.018	0.290 ± 0.023	0.333
3	-0.318 ± 0.018	-0.184 ± 0.018	-0.248 ± 0.021	-0.333
4	0.417 ± 0.012	0.385 ± 0.017	0.381 ± 0.022	0.500
5	-0.541 ± 0.019	-0.581 ± 0.028	-0.682 ± 0.022	-1.000
6	0.735 ± 0.013	0.689 ± 0.018	0.764 ± 0.022	1.000
7	-0.296 ± 0.015	-0.259 ± 0.022	-0.349 ± 0.022	-0.500

Table 7: Average values of P_z obtained from the EDDA measurements prior to our experiment at lower energies and intensities. These are compared to the values obtained from the $\vec{d}p \to dp$ reaction using the values of P_{zz} deduced from our $\vec{d}p \to (pp)n$ and $\vec{d}p \to {}^3\mathrm{He}\,\pi^0$ measurements.

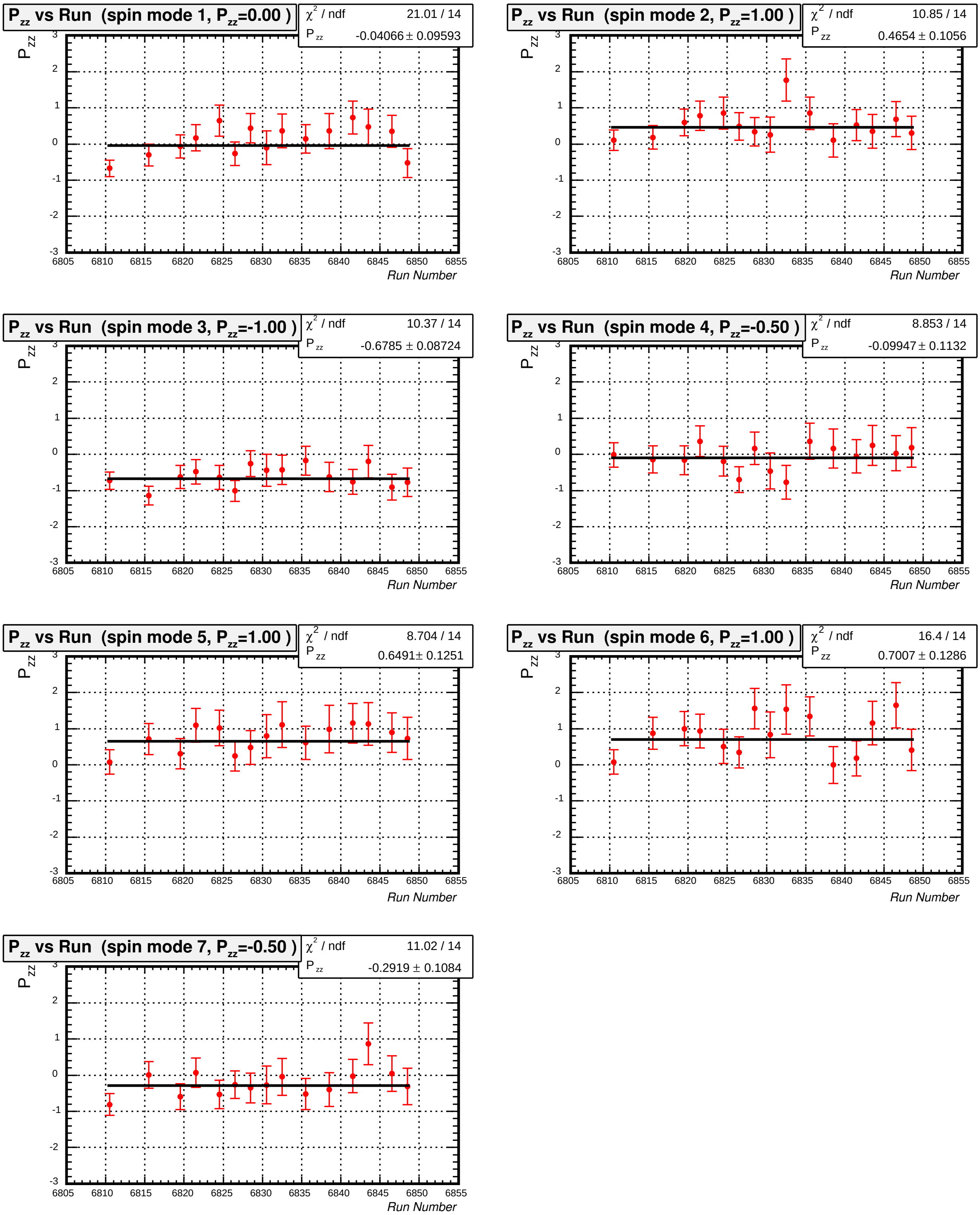

Figure 22: The results of the P_{zz} measurement run by run in the November 2003 beam time using the $\vec{d}p \to {}^3\mathrm{He}\,\pi^0$ reaction. ($\theta_{^3\mathrm{He}} < 1.6^\circ$)

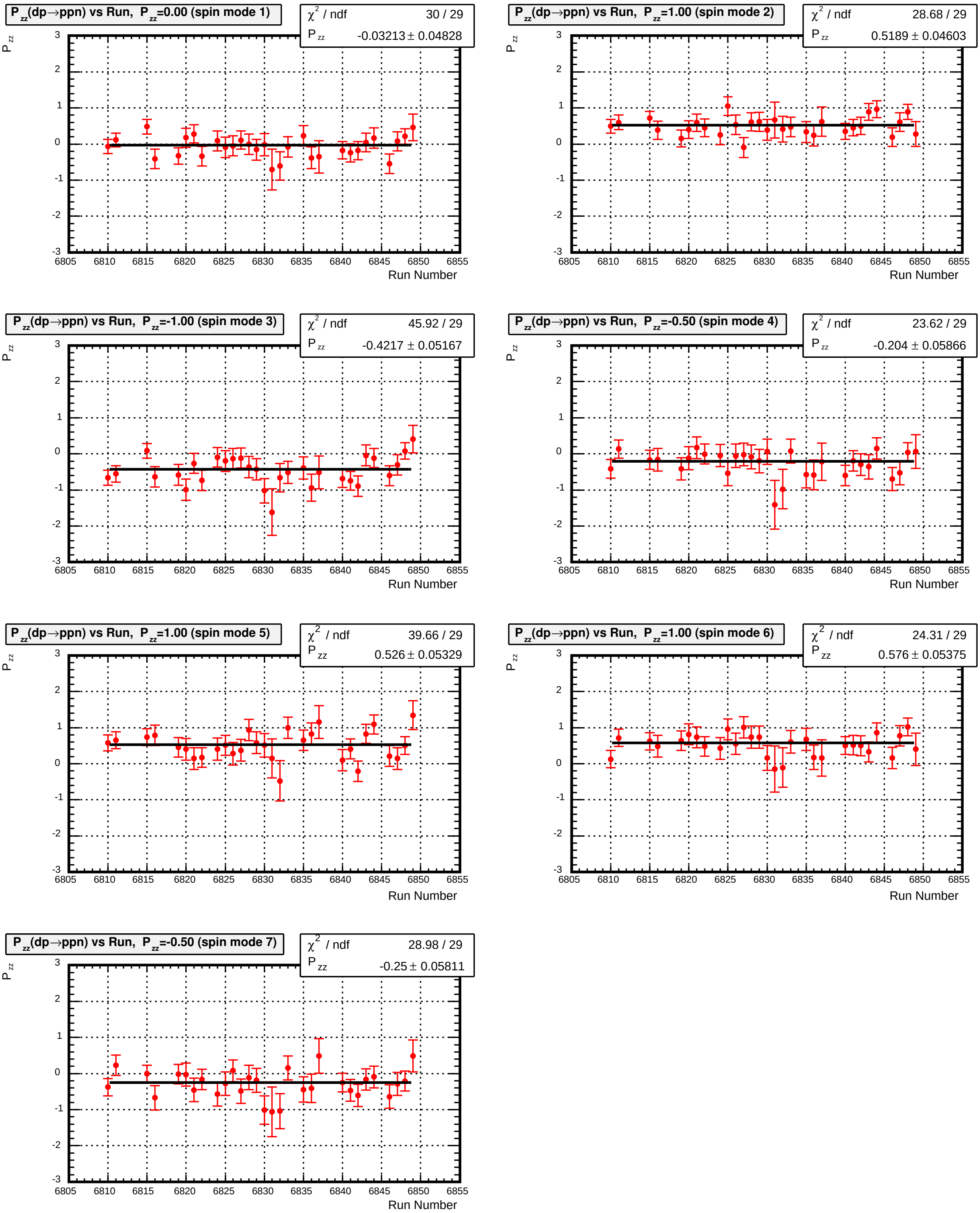

Figure 23: The results of the P_{zz} measurement run by run in the November 2003 beam time using the $\vec{d}p \to (2p)n$ reaction. ($\theta_{(2p)} < 1.2^\circ$)

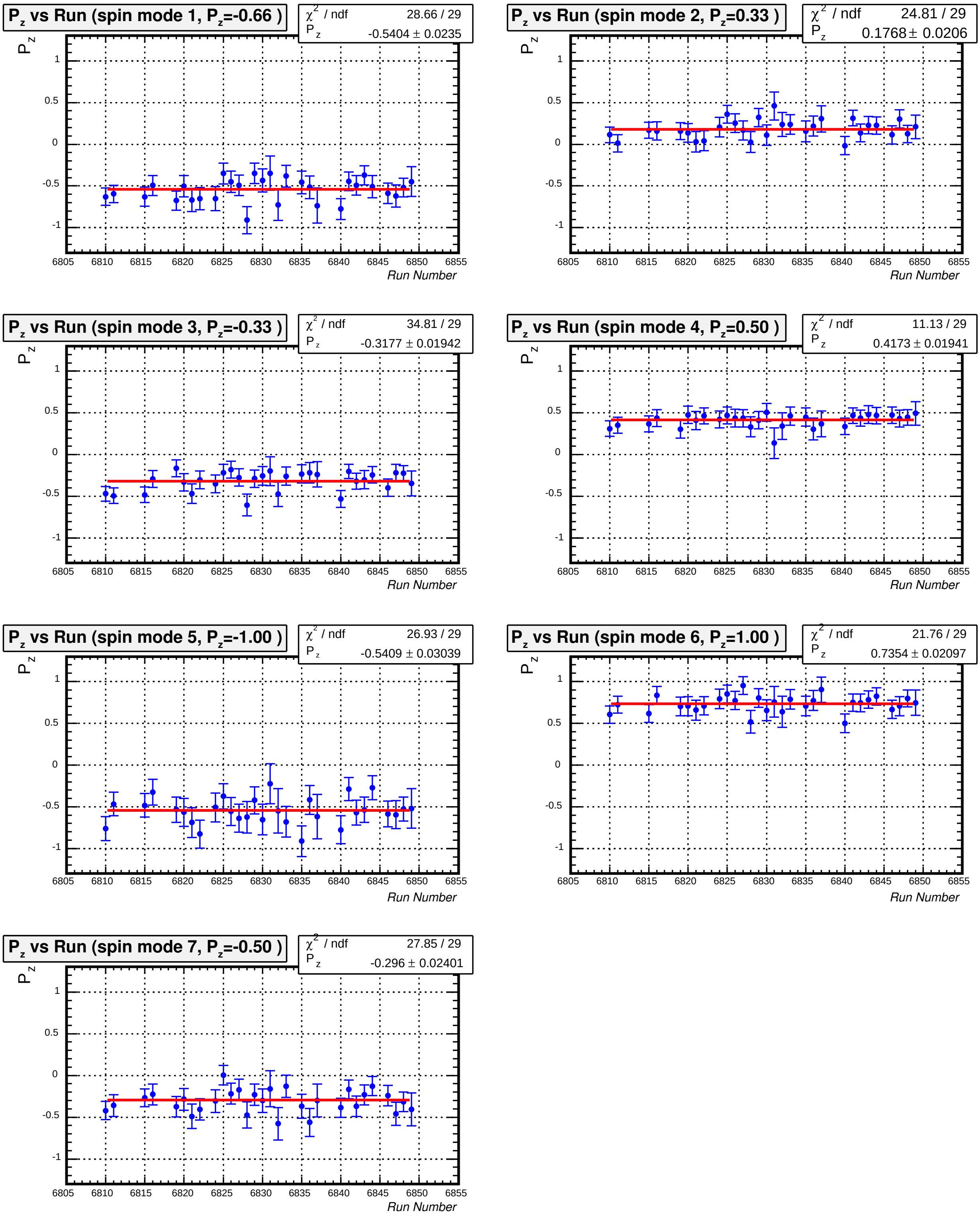

Figure 24: The results of the P_z measurement run by run in the November 2003 beam time using the $\vec{d}p \to dp$ reaction.

6.6 Analysing power (T_{20}) of the charge-exchange reaction

The method and assumptions are similar to those used for the P_{zz} calculation (see Sec. 6.3). The counts belonging to the $\vec{d}p \to (pp)_{^1S_0} + n$ reaction with the final proton pair produced near zero degrees with small excitation energy ($E_{pp} < 2$ MeV) were identified. Taking the beam tensor polarization (P_{zz}) determined from the polarimetry reaction, we can use the ratios of the number of events recorded for different spin states of the beam. The final expression used for the T_{20} determination (assuming that the T_{22} tensor analysing power is small), can be written in the form:

$$T_{20} = \frac{2\sqrt{2}}{P_{zz}} \left[\frac{d\sigma_\circ}{d\Omega}(\vartheta) - \frac{d\sigma^\uparrow}{d\Omega}(\vartheta) \right] \Big/ \frac{d\sigma_\circ}{d\Omega}(\vartheta) \,.$$

Using the extracted counts of the $\vec{d}p \to (pp)_{^1S_0} + n$ reaction normalized to the BCT counts, we get the results for T_{20} run by run that are shown in Fig. 25. For the average value of T_{20} from these four spin modes we get: $T_{20} = 0.38 \pm 0.10$, which coincides well with the predicted value of 0.42 [7].

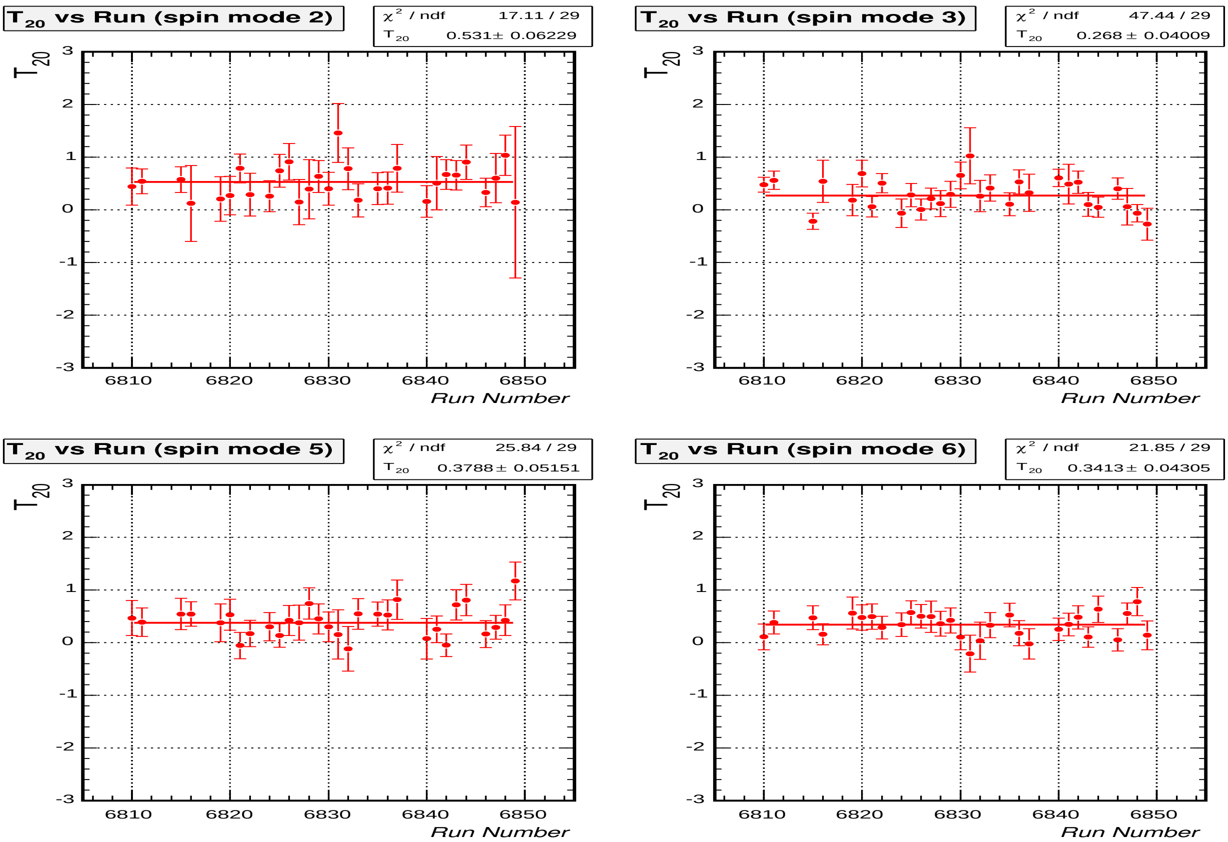

Figure 25: Results of the T_{20} measurement for the $\vec{d}p \to (pp)_{^1S_0} + n$ charge-exchange reaction.

7 Conclusion

7.1 Summary

The data analysis from the 60 hours of 1.2 GeV polarized deuteron beam time taken in November 2003 is not yet completely finished, but, we have achieved the following:

- Measured $\vec{d}p \to$ single and double-track events in ANKE and clearly identified, amongst others, the $\vec{d}p \to dp$, $\vec{d}p \to {}^3\mathrm{He}\,\pi^0$, and $\vec{d}p \to (pp)n$ reactions;

- Determined the luminosity in the experiment by comparing to published deuteron-proton elastic scattering cross sections, which have a precision of about 10%;

- Obtained differential distributions for the $\vec{d}p \to (pp)n$ reaction as functions of the momentum transfer t and the pp excitation energy E_{pp};

- Worked with eight different combinations of vector (P_z) and tensor (P_{zz}) deuteron polarizations provided by the ion source and accelerated in COSY;

- Extracted values of P_{zz} by measuring the polarization dependence of the small angle $\vec{d}p \to {}^3\mathrm{He}\,\pi^0$ count rates and using the T_{20} analysing power, known with high precision from Saclay measurements;

- Extracted values of P_{zz} by comparing the polarization dependence of the $\vec{d}p \to (pp)n$ reaction for small pp excitation energies with the predictions of the undistorted Bugg & Wilkin model, which describes well data published at lower and higher energies;

- Compared our two values of P_{zz} for the six non-zero source spin states with the values obtained <u>before</u> our run by EDDA at <u>lower</u> energies and <u>lower</u> source intensities. Although there is qualitative agreement, the variations for the individual spin states are bigger than expected on the basis of the statistics achieved, suggesting that the systematics of both our and the EDDA measurements must be studied further. Nevertheless the mean value over all states is reasonable: $P_{zz}({}^3\mathrm{He}\pi^0)/P_{zz}(\mathrm{EDDA}) = 0.96 \pm 0.21$, where the error is determined purely from the spread in the individual results;

- Using the values of P_{zz} from the ${}^3\mathrm{He}\,\pi^0$ final state in conjunction with our $\vec{d}p \to dp$ elastic scattering data, the deduced values of the deuteron vector polarization P_z are in reasonable agreement with the EDDA values, though again with a spread over different source states that is larger than expected on the basis of statistical errors, which are comparatively small. The mean value is $P_z({}^3\mathrm{He}\pi^0)/P_z(\mathrm{EDDA}) = 1.03 \pm 0.15$.

- Using the measured values of P_{zz} from the $\vec{d}p \to {}^3\mathrm{He}\,\pi^0$ reaction, we deduce that for the deuteron charge exchange reaction $T_{20} = 0.38 \pm 0.10$, to be compared to the Bugg & Wilkin prediction of 0.42.

7.2 Outlook

The $\vec{d}\vec{p}$ spin–correlation studies envisaged in the continuation necessitate the availability of a polarized hydrogen target. For such experiments a polarized internal target (PIT) is presently being prepared [22]. The PIT consists of a storage cell fed by an atomic beam source (ABS) [39] and a Lamb Shift Polarimeter (LSP) [40] for the measurement of the target polarization.

The development of the ABS for ANKE has been finalized. Beam intensities of 7.8×10^{16} hydrogen atom per second in two hyperfine states have been reached with a polarization of about 90%. For deuterium, where somewhat lower preliminary values have been reached until now, final tuning has to be done.

The LSP will be used to measure and monitor the nuclear polarization of the target gas by removing a small fraction (about 10^{-4}) of the gas by sample tube. The final development of LSP itself has been performed with the use of the direct ABS beam. With the full ABS beam intensity of 7.8×10^{16} $\vec{\mathrm{H}}$ atoms/s, the polarization is measured within 2 s with an accuracy better 1%. At present studies are being performed with the LSP positioned at a test set-up of feeding, storage, and sampling tubes made from teflon [41].

First tests of storage cell at ANKE have been done to estimate the beam size at the ANKE target position since, before these tests, the size of the COSY beam at injection and after acceleration was rather uncertain. These findings are needed to build the storage cells for the polarized target and, depending on the size of the cells, determine how much beam will be lost at injection, and also determine the target density. The cell tests will be continued in summer of 2004. In the same time a test mounting of PIT prior to installation at ANKE is planned. A first commissioning experiment with PIT is planned in a frame of the deuteron breakup charge exchange experimental program [8]

Appendix A. Kinematics of the $dp \to (pp)n$ reaction

In this chapter the kinematics of the process $dp \to (pp)n$ is discussed. In order to describe a reaction with two initial particles and three particles in the final state ($A + B \to 1 + 2 + 3$) one has to define $3 \times (2+3)$ components of momenta. The momentum–energy conservation laws define four relations between the momentum components of initial and final particles. In addition, the choice of c.m. system allows one to use three conditions for the initial particles $\boldsymbol{p}_A^{c.m.} + \boldsymbol{p}_B^{c.m.} = 0$ and three conditions for the particles in the final state $\boldsymbol{p}_1^{c.m.} + \boldsymbol{p}_2^{c.m.} + \boldsymbol{p}_3^{c.m.} = 0$. Therefore, the reaction is defined by $3 \times (2+3) - 4 - 3 - 3 = 5$ independent variables. For the description of the deuteron breakup reaction $pd \to (pp)n$ the following ones are used: excitation energy of the two protons E_{pp}, polar angle $\theta_{pp}^{c.m.}$ and azimuthal angle $\phi_{pp}^{c.m.}$ of proton pair in c.m. system, polar angle $\theta_k^{c.m.}$ and azimuthal angle $\phi_k^{c.m.}$ of the protons in the rest frame of the proton pair relative to the direction of the proton pair in c.m. system (Fig. 26). The analysing power is expressed in terms of the neutron scattering angle $\theta_n^{c.m.} = \pi - \theta_{pp}^{c.m.}$.

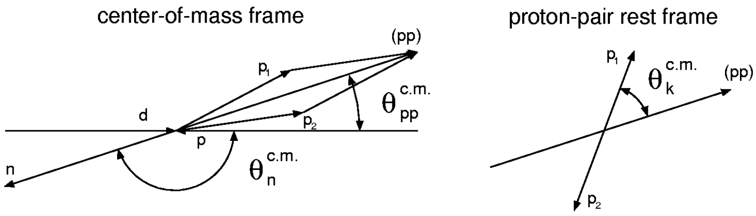

Figure 26: Momentum vectors of reactions $pd \to (pp)n$ in the centre–of–mass system and the rest frame of the two protons.

The excitation energy of the proton pair is defined as

$$E_{pp} = \sqrt{(E_{p_1} + E_{p_2})^2 - (\vec{p}_{p_1} + \vec{p}_{p_2})^2} - 2m_p,$$

where E_{p_1}, E_{p_2} are total energies and $\vec{p}_{p_1}$, $\vec{p}_{p_2}$ are the 3–momenta of the protons, m_p is the proton mass. The excitation energy E_{pp} is invariant under Lorentz transformation. From the measured 3–momenta of the two protons the missing mass of the neutron can be calculated from

$$M_{miss} = \sqrt{(E_p + m_d - E_{p_1} - E_{p_2})^2 - (\vec{p}_p - \vec{p}_{p_1} - \vec{p}_{p_2})^2}.$$

7.3 Acknowledgements

I would like to thank:

- Prof. C. Wilkin who has spent hours and hours reading this thesis as my referee, and giving useful advice in physical topics.
- Prof. H. Ströher who provided the possibility to do this work at the Institute, and was allways ready for help.
- Dr. F. Rathmann and Dr. A. Kacharava for continuous advice day and night, many fruitful discussions and contributions. I learned a lot from them, it was realy good lesson for me.
- Prof. M. Nioradze whit whom we started to prepare for this work, and who gave the first push.
- All my colleagues from the ANKE collaboration.
- My parents deserves credit for keeping up with me under all circumstances.

References

[1] J. Bystricky et al., Nucl. Phys. A444 (1985) 597.

[2] R.A. Arndt et al., Phys. Rev. C62 (2000) 034005.

[3] M. Altmeier et al., Phys. Rev. Lett. 85 (2000) 1819.

[4] R.A. Arndt et al., Phys. Rev. C50 (1994) 2731;C56 (1997) 3005.

[5] A. de Lesquen et al., Eur. Phys. J C11 (1999) 69.

[6] D.V. Bugg and C. Wilkin, Phys. Lett. B152 (1985) 37.

[7] D.V. Bugg and C. Wilkin, Nucl. Phys. A467 (1987) 575.

[8] A. Kacharava et al., 'The polarized charge-exchange reaction', COSY proposal # 125, Spokesperson: A. Kacharava, F. Rathmann (2003).

[9] G.C. Ohlsen, Rep. Prog. Phys. 35 (1972) 717-801.

[10] W. Haeberli, Ann. Rev. Nucl. Part. Sci, **17**, 373 (1967).

[11] B. Braun, PhD-Thesis, Fakultät für Physik, Ludwig-Maximilians-Universität, München; English translation (Thesis 95-047) available from `www-library.desy.de/preprints.html#diss`

[12] R.J. Philpott, Nucl. Instr. and Meth. **A259**, 317 (1987).

[13] K. Yonehera et al., AIP Conf. Proc. 698 (2003) 763.

[14] A. Lehrach *et al.*, Annual Report IKP 1997.

[15] R. Maier, NIM **A 390** (1997) 1.

[16] P. D. Eversheim *et al.*, The Polarized Ion–Source for COSY, Proc. International Symposium on High Energy Spin Physics SPIN 1996, Amsterdam (1996), published in World Scientific Singapore (1997).

[17] D. Prasuhn *et al.*, NIM **A 441** (2000) 167.

[18] D. Prasuhn *et al.*, Cooling at COSY, Workshop on Beam Cooling and Related Topics, Bad Honnef 2001, FZ Jülich, Matter and Material, V. **13**, ISBN 3-89336-316-5.

[19] S. Barsov et al., Nucl. Instr. Meth. A462 (2001) 364.

[20] A. Khoukaz *et al.*, Eur. Phys. J. **D 5** (1999) 275.

[21] V. Balanutsa *et al.*, IKP FZ–Jülich Annual Report 2001, Jül–3978, Jülich, 2002.

[22] F. Rathmann *et al.*, Proc. of the 15^{th} Int. Spin Physics Symposium, BNL, New York, 2002, AIP 0-7354-0136-5/03 (2003) 553.

[23] V. Kleber *et al.*, Phys. Rev. Lett. **91** (2003) 172304.

[24] S. Barsov *et al.*, COSY Proposal #114, 2002, spokesperson: R. Schleichert.

[25] M. Büscher *et al.*, COSY Proposal #94, 2000, spokesperson: A. Khoukaz.

[26] V. Komarov *et al.* COSY Proposal #20 (1999), Spokespersons: V. Komarov, F. Rathmann.

[27] B. Chiladze *et al.*, Part. Nucl., Lett. **4** (2002) 95.

[28] S. Dymov *et al.*, Part. Nucl., Lett. **2** (2004) 40.

[29] V. Komarov et al., Phys. Lett. B553 (2003) 179.

[30] S. Barsov et al., submitted to Nucl. Instr. Meth.

[31] I. Lehmann *et al.*, to be published in NIM **A**.

[32] S. Barsov *et al.*, to be published in EPJ **A**.

[33] C. Kerboul, Phys. Lett. 181B (1986) 28.

[34] N. Katayama et al. Nucl. Phys. A438 (1985) 685.

[35] M. Marshak et al., Phys. Rev. C18 (1978) 1.

[36] V. Glagolev et al., VII Symposium on Spin Phenomena, Protvino, Sept.86, 1987, p.146 (JINR preprint P1-88-6)

[37] J. Arvieux et al., Nucl. Instr. Meth. A273 (1988) 48.

[38] J. Arvieux et al., Nucl. Phys. A431 (1984) 613.

[39] M. Mikirtytchiants et al., Proc. of Int. Workshop on Polarized Sources and Targets, Nashville, Indiana, USA, 2001. ISBN 981-02-4917-9, p. 47.

[40] R. Engels *et al.*, Rev. Sci. Instr. **74** (2003) 4607.

[41] R. Engels *et al.*, IKP FZ–Jülich Annual report 2003, Jül–4107, Jülich, 2004.

[42] G. Borchert *et al.*, IKP FZ–Jülich Annual Report 1997, Jül-3505, Jülich, 1998, p. 59.